Journal of Computational Physics **174,** 816–851 (2001)
doi:10.1006/jcph.2001.6939, available online at http://www.idealibrary.com on IDEAL®

Revisiting Numerical Errors in Direct and Large Eddy Simulations of Turbulence: Physical and Spectral Spaces Analysis

Ivan Fedioun,*,[1] Nicolas Lardjane,† and Iskender Gökalp†

*L.M.E./E.P.E.E., E.S.E.M. Université d'Orléans, 8, rue Léonard de Vinci, 45072 Orleans Cedex 2, France; and
†L.C.S.R./E.P.E.E., C.N.R.S. Orléans, 1c, avenue de la Recherche Scientifique, 45071 Orleans Cedex 2, France
E-mail: Ivan.Fedioun@univ-orleans.fr, lardjane@cnrs-orleans.fr, and gokalp@cnrs-orleans.fr

Received September 25, 2000; revised July 18, 2001

Some recent studies on the effects of truncation and aliasing errors on the large eddy simulation (LES) of turbulent flows via the concept of modified wave number are revisited. It is shown that all the results obtained for nonlinear partial differential equations projected and advanced in time in spectral space are not straightforwardly applicable to physical space calculations due to the nonequivalence by Fourier transform of spectral aliasing errors and numerical errors on a set of grid points in physical space. The consequences of spectral static aliasing errors on a set of grid points are analyzed in one dimension of space for quadratic products and their derivatives. The dynamical process that results through time stepping is illustrated on the Burgers equation. A method based on midpoint interpolation is proposed to remove in physical space the static grid point errors involved in divergence forms. It is compared to the sharp filtering technique on finer grids suggested by previous authors. Global performances resulting from combination of static aliasing errors and truncation errors are then discussed for all classical forms of the convective terms in Navier–Stokes equations. Some analytical results previously obtained on the relative magnitude of subgrid scale terms and numerical errors are confirmed with 3D realistic random fields. The physical space dynamical behavior and the stability of typical associations of numerical schemes and forms of nonlinear terms are finally evaluated on the LES of self-decaying homogeneous isotropic turbulence. It is shown that the convective form (if conservative properties are not strictly required) associated with highly resolving compact finite difference schemes provides the best compromise, which is nearly equivalent to dealiased pseudo-spectral calculations.

Key Words: large eddy simulation; numerical errors; Stability; dealiasing techniques; Navier–Stokes equations; turbulence; finite difference; modified wave number; pseudo-spectral discretization; self-decaying homogeneous isotropic turbulence.

[1] Corresponding author. Fax: 33-(0)2-38-41-73-83.

0021-9991/01 $35.00

INTRODUCTION

Numerical simulations of turbulent flows are mainly performed in two ways: For theoretical studies leading to fundamental knowledge of the physics of these flows and then to different modeling issues, spectral methods are best suited because of their extreme accuracy and their well-established dealiasing techniques [2]. On the other hand, for high speed turbulent flows such as supersonic mixing of reactants or for complex flow geometries, one has to work in physical space with finite difference or finite volume methods. Finite volumes are best suited for industrial Reynolds averaged Navier–Stokes simulations (RANS) with unstructured meshes, whereas finite differences are mainly used in the direct numerical simulation (DNS) or large eddy simulation (LES) approaches, since higher order accuracy is easier to achieve. Higher order methods are required in DNS or LES because a wide range of scales has to be properly represented. The resolution required for the accurate representation of the smallest scales is linked to the numerical errors produced by the discretization of the governing equations and is discussed in [12].

A couple of years ago, our team performed the DNS of the 2D compressible temporal mixing layer. Navier–Stokes equations were solved for conservative variables, with the nonlinear convection terms cast in conservation (or divergence) form, and the viscous terms in nonconservation form:

$$\frac{\partial \mathbf{U}}{\partial t} + \frac{\partial \mathbf{F}}{\partial x} + \frac{\partial \mathbf{G}}{\partial y} = \mathbf{V}.$$

Sixth-order compact schemes [7] were used for spatial discretization, and a third-order low storage Runge–Kutta scheme was used for time stepping. Boundary conditions were periodic in the streamwise direction and nonreflecting (NSCBC) [17] in the transverse direction. The Reynolds number based on the free stream velocities and the initial vorticity thickness δ was 200. The convective Mach number was 0.576. Discretization was 192×256 grid points in a $45\delta \times 50\delta$ computational domain. At dimensionless time $t = 60$, the calculation became unstable (Fig. 1a).

Performing the same calculation with equations cast in convective form,

$$\frac{\partial \mathbf{U}}{\partial t} + [A]^F \frac{\partial \mathbf{U}}{\partial x} + [A]^G \frac{\partial \mathbf{U}}{\partial y} = \mathbf{V}; \qquad [A]^F_{ij} = \frac{\partial F_i}{\partial U_j},$$

showed no sign of instability (Fig. 1b), and the integration could proceed until saturation of the temporal box. Since the only change was in the form of nonlinear terms, we concluded that the convective form had a better long-time behavior than the divergence one due to a lower level of numerical errors (combination of discretization and aliasing errors).

The theoretical analysis of discretization errors for first or higher derivation schemes has received renewed interest since publication of the famous paper by Lele [7], who focused on the *resolving efficiency* rather than on the formal accuracy of the discrete schemes by means of the modified wave number (MWN). The computational efficiency, i.e., the operation count for a given well-resolved shortest scale, has then been emphasized, both for linear (e.g., [3]) and nonlinear problems [4]. Another source of numerical error arises from the nonconservation of transported variables by some discrete operators, which may violate the physical conservation laws. Higher order schemes which conserve mass, momentum, and kinetic energy in a discrete sense have been recently designed for uniform [14] and extended to nonuniform [18] grids.

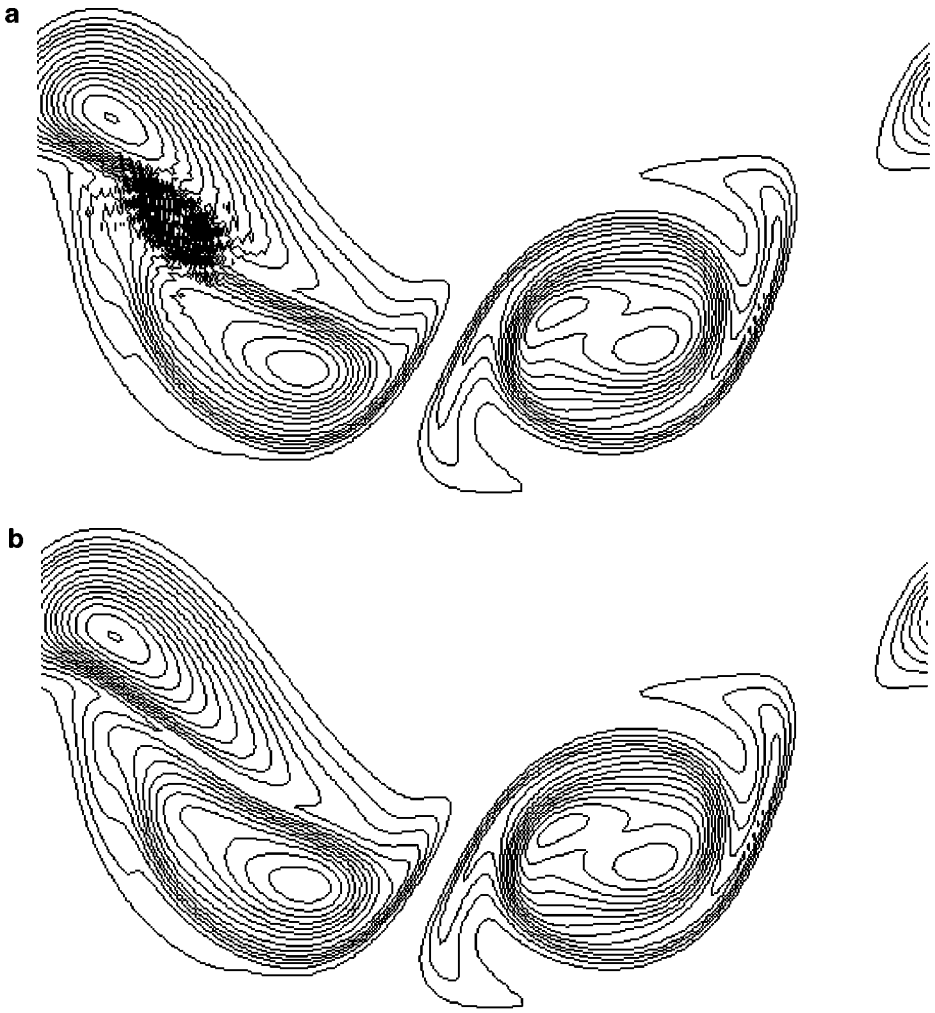

FIG. 1. Conservative variables. (a) divergence form; (b) convective form.

Nevertheless, the problem of aliasing errors for nonlinear partial differential equations (PDEs) advanced in physical space with finite difference schemes, although mentioned by Lele [7], has not been clearly formulated. The reason is perhaps that in the past two decades, many studies on the effects of aliasing errors have been conducted in the framework of spectral methods (e.g., [13]), by analyzing the dynamical behavior of aliased and dealiased calculations, i.e., their differences in time evolution. The major issue was to compare the different forms of the nonlinear terms in Navier–Stokes equations projected in spectral space and their respective stability properties. In the same spirit, a previous study [6] mimicked the physical space behavior of finite differences for both aliasing and truncation errors. That is, pseudo-spectral codes were used with the MWN of the scheme to be tested instead of the spectral wave number in derivatives, and with or without dealiasing. Results were then extrapolated to physical space calculations. In fact, this is not straightforward and may lead to erroneous conclusions for aliasing errors, and for combination of aliasing and truncation errors, mainly in LES applications where the spectral contents of the simulated

fields still have significant energy at the cutoff. For instance, the authors concluded that the skew-symmetric form produces the lowest level of aliasing errors, which is true for the pseudo-spectral projection of Navier–Stokes equations but is not true when implemented in physical space. This kind of confusion occurs frequently in the literature (e.g., [1]) and has been the motivation for the present study. The following issues are addressed here:

(i) What are the consequences, through inverse Fourier transform on a set of grid points in physical space, of dealiasing the Fourier coefficients of a quadratic product?

(ii) What is the error introduced on a set of grid points in physical space for the finite difference derivative of a spectrally aliased or dealiased quadratic product?

(iii) Are the spectral space projection and time advancement of a nonlinear PDE, with MWNs substituted for spectral wave numbers in derivatives, of any help in analyzing the behavior of finite difference schemes implemented in physical space and advanced in time for this PDE?

(iv) Is it possible to derive some numerical techniques to minimize numerical errors for PDEs solved in physical space and what would be their computational cost?

(v) What kind of dynamical error results in physical space through time advancement of a nonlinear PDE cast in divergence or convective form in case of marginal resolution, and what are the conservation properties of the whole process?

(vi) In reference to (iii), what should be the correct procedure, using a pseudo-spectral code, to analyze the relative magnitude of discretization errors and subgrid terms in the LES of turbulent flows, and does the numerical experiment confirm some previous analytical results [4]?

In the first section, we will recall briefly the concept of MWN to address items (i), (ii), and (iii) in one dimension of space. Item (iv) will then be discussed for filtering and interpolation techniques. The viscous Burgers equation will be a test case for item (v).

The second section will be devoted to item (vi). The suitable procedure to analyze the static numerical errors introduced in the spatial discretization of filtered Navier–Stokes equations will be explained. Error spectra will be presented for a realistic 3D pseudo-random velocity field typical of the LES of isotropic turbulence and compared to the subgrid scale term computed with the spectral eddy viscosity model of Lesieur and Metais [11]. This point is a numerical checking of some analytical bounds given by Ghosal [4], although his results should apply to spectral projection of Navier–Stokes equations rather than to physical space implementation of the numerical schemes. Finally, a dynamical study will show the effect of numerical errors on the stability of self-decaying isotropic turbulence LES. The physical space behavior of second-order centered and fourth-order spectral-like compact schemes will be mimicked for convective and divergence forms of the nonlinear terms and compared to a dealiased pseudo-spectral simulation.

1. TRUNCATION, ALIASING, AND GRID ERRORS FOR NONLINEAR TERMS IN PHYSICAL SPACE

In this section, we will use discrete Fourier transforms (DFTs) rather than the continuous one in analytical developments, since the numerical experiments to be presented in Section 2 are implemented that way.

1.1. *Basic Concepts—Notations*

We consider a uniform grid of $N+1$ points $x_i,\ i=0,\ldots,N$ in physical space, discretizing a compact support $x \in [0, L]$ ($L = 2\pi$ for simplicity) on which a periodic function $u(x)$ is defined and is represented by the set of the discrete values $u^N = \{u_i^N;\ i = 0,\ldots,N-1\}$. The discrete Fourier transform of u is given by its $N/2$-degree trigonometric interpolant

$$I_N u(x_i) = u_i^N = \sum_{k=-N/2}^{N/2-1} \tilde{u}_k^N e^{j_c \frac{2\pi}{N} ik}, \tag{1}$$

$$\tilde{u}_k^N = \frac{1}{N} \sum_{i=0}^{N-1} u_i^N e^{-j_c \frac{2\pi}{N} ik}. \tag{2}$$

1.1.1. Modified wave number. Applying discrete first D_i^1 and second D_i^2 derivation operators to (1) introduces modified wave numbers in the discrete representations of du/dx and d^2u/dx^2 built from u^N,

$$\left.\frac{du}{dx}\right|_i \approx D_i^1(I_N u) = \sum_{k=-N/2}^{N/2-1} j_c k'(\omega_k) e^{j_c \frac{2\pi}{N} ik}, \tag{3}$$

$$\left.\frac{d^2u}{dx^2}\right|_i \approx D_i^2(I_N u) = \sum_{k=-N/2}^{N/2-1} -k''(\omega_k) e^{j_c \frac{2\pi}{N} ik}, \tag{4}$$

where $\omega_k = k\frac{2\pi}{L}\Delta x$. After applying the scaling, we obtain

$$\omega'(\omega_k) = \Delta x\ k'(\omega_k), \tag{5a}$$

$$\omega''(\omega_k) = \Delta x^2 k''(\omega_k). \tag{5b}$$

Equations (5) give the resolving efficiencies of the schemes, independently of grid size; e.g., for the second-order centered finite difference scheme, $\omega'(\omega_k) = \sin(\omega_k)$. For a spectral-like compact first-derivative pentadiagonal scheme [7],

$$\begin{aligned} &\beta\left(u'^N_{i+2} + u'^N_{i-2}\right) + \alpha\left(u'^N_{i+1} + u'^N_{i-1}\right) + u'^N_i \\ &\quad = c\frac{u_{i+3}^N - u_{i-3}^N}{6\Delta x} + b\frac{u_{i+2}^N - u_{i-2}^N}{4\Delta x} + a\frac{u_{i+1}^N - u_{i-1}^N}{2\Delta x}, \end{aligned} \tag{6}$$

the reduced modified wave number is

$$\omega'(\omega_k) = \frac{a\sin(\omega_k) + (b/2)\sin(2\omega_k) + (c/3)\sin(3\omega_k)}{1 + 2\alpha\cos(\omega_k) + 2\beta\cos(2\omega_k)}, \tag{7}$$

and the scheme at sixth-order may be tuned to produce about 80% of resolving efficiency at 0.001 relative error. Since these schemes are centered, their MWNs are real and the error is purely dispersive.

1.1.2. Aliasing. The term "aliasing" appears usually in the framework of pseudo-spectral evaluation of convolution sums [2]. Let $w = uv$. Estimating the coefficients of $I_N w$ pseudo-spectrally, i.e., by discrete Fourier transform of the point-wise product $(u_i^N v_i^N)$,

$$I_N w(x_i) = w_i^N = \sum_{k=-N/2}^{N/2-1} \tilde{w}_k^N e^{j_c \frac{2\pi}{N} ik}, \tag{8}$$

$$\tilde{w}_k^N = \frac{1}{N} \sum_{i=0}^{N-1} u_i^N v_i^N e^{-j_c \frac{2\pi}{N} ik}, \tag{9}$$

gives

$$\tilde{w}_k^N = \sum_{n=-N/2}^{N/2-1} \tilde{u}_n^N \tilde{v}_{k-n}^N + \sum_{n=-N/2}^{N/2-1} \tilde{u}_n^N \tilde{v}_{k-n\pm N}^N, \qquad k = -N/2, \ldots, N/2-1. \tag{10}$$

So, although its Fourier coefficients are contaminated by an aliasing error—the second sum in (10)—the discrete product is exact at grid nodes in physical space. If dealiasing is performed for (10) by the 3/2 rule or phase shift, transforming $\tilde{w}_k^N$ back into physical space will not give $w_i^N = u_i^N v_i^N$ at the grid points. The reason is that the discrete Fourier transform (8) has bounded up to $\pm N/2$ modes the possibly $\pm N$ modes which could have been computed in a straightforward calculation of the convolution sum:

$$(\tilde{u}^N * \tilde{v}^N)_k = \sum_{n+m=k} \tilde{u}_n^N \tilde{v}_m^N, \qquad n, m = -N/2, \ldots, N/2-1. \tag{11}$$

So, we can consider (11) as the coefficients

$$\tilde{w}_k^{2N} = \frac{1}{2N} \sum_{j=0}^{2N-1} w_j^{2N} e^{-j_c \frac{2\pi}{2N} jk}, \qquad k = -N, \ldots, N-1, \tag{12}$$

of the N-degree trigonometric interpolant

$$I_{2N} w(\bar{x}_j) = w_j^{2N} = \sum_{k=-N}^{N-1} \tilde{w}_k^{2N} e^{j_c \frac{2\pi}{2N} jk}, \qquad j = 0, \ldots, 2N-1, \tag{13}$$

of $w(x)$ at the nodes $\bar{x}_j$ of a double density uniform physical grid

$$\begin{cases} \bar{x}_{2i} = x_i \quad i = 0, \ldots, N \\ \bar{x}_{2i+1} = (x_{i+1} + x_i)/2, \end{cases}$$

which could be estimated by the point-wise product $(u_j^{2N} v_j^{2N})$ of the (exactly) interpolated values of u and v at the nodes $\bar{x}_j$ from their values at the nodes x_i. So, in physical space, the difference

$$e(x) = I_N w(x) - I_{2N} w(x) \tag{14}$$

may be written at the nodes $x_i = \bar{x}_{2i}$ as

$$e_i = \sum_{k=-N/2}^{N/2-1} \left(\sum_{n=-N/2}^{N/2-1} \tilde{u}_n^N \tilde{v}_{k-n\pm N}^N \right) e^{j_c \frac{2\pi}{N} ik} \quad \text{(I)}$$

$$- \left\{ \sum_{k=-N}^{-N/2-1} \left(\sum_{n=-N/2}^{N/2-1} \tilde{u}_n^N \tilde{v}_{k-n}^N \right) e^{j_c \frac{2\pi}{2N} 2ik} + \sum_{k=N/2}^{N-1} \left(\sum_{n=-N/2}^{N/2-1} \tilde{u}_n^N \tilde{v}_{k-n}^N \right) e^{j_c \frac{2\pi}{2N} 2ik} \right\} \quad \text{(II)} \tag{15}$$

and is, of course, zero at these points by definition. So, the aliasing error (I) in the pseudo-spectral estimation (9) and (10) takes the same values at the physical grid points as the error (II) due to the bounding of (11) up to $|k| = k_c = N/2$. Both will vanish if the wave number content of u and v is zero for modes greater than $N/4$ (what we call "marginal resolution"), simply because in this case, the N-point grid can capture all of the $N/2$ modes of the product (uv). *This answers item (i).*

1.1.3. Aliasing and derivative errors. Let us apply a discrete D_i^1 derivation operator to (15). It gives readily

$$D_i^1(e) = \sum_{k=-N/2}^{N/2-1} \left(j_c k'(\omega_k) \sum_{n=-N/2}^{N/2-1} \tilde{u}_n^N \tilde{v}_{k-n\pm N}^N \right) e^{j_c \frac{2\pi}{N} ik} \quad \text{(I)}$$

$$- \left\{ \sum_{k=-N}^{-N/2-1} \left(j_c k'(\omega_k) \sum_{n=-N/2}^{N/2-1} \tilde{u}_n^N \tilde{v}_{k-n}^N \right) e^{j_c \frac{2\pi}{N} ik} \right.$$

$$\left. + \sum_{k=N/2}^{N-1} \left(j_c k'(\omega_k) \sum_{n=-N/2}^{N/2-1} \tilde{u}_n^N \tilde{v}_{k-n}^N \right) e^{j_c \frac{2\pi}{N} ik} \right\}. \quad \text{(II)} \tag{16}$$

This is precisely the kind of static error introduced at grid points by the *divergence form* implemented with a finite difference scheme in physical space, in case of marginal resolution. This error occurs only through spatial differentiation of a discrete product, the product itself being exact at grid nodes. It is emphasized by the resolving efficiency of the derivation scheme. If dealiasing is performed for Fourier coefficients of the quadratic product before transforming back to physical space, part (II) of the error will still be at the grid nodes. On the other hand, the convective form does not produce such an error. *This answers item (ii).* Let us illustrate this with a simple example.

Consider $u(x) = \sin(15x)$ and $w(x) = u^2(x) = \frac{1}{2}(1 - \cos(30x))$. On a $N = 32$ point grid, mode 30 will alias mode -2. So, $I_N w$ looks like a $k = -2$ wave. If differentiation of $I_N w$ is performed exactly, the result will be very different from $I_N dw/dx$ (Fig. 2).

1.2. *Physical Space versus Spectral Space Simulations*

The question addressed in this section is the equivalence between calculations advanced in physical space with finite difference schemes and calculations advanced in spectral space with MWN of the schemes, dealiased or not.

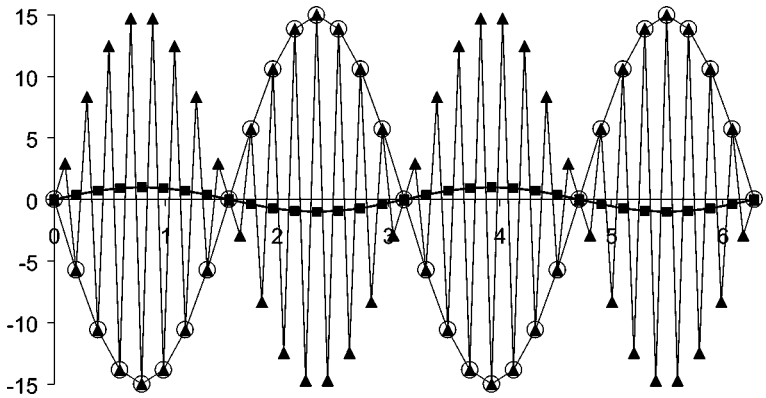

FIG. 2. Derivative of a discrete product. ⊖, $I_N dw/dx$; ▲, $I_{2N} dw/dx$; ■, $d(I_N W)/dx$.

First, one has to distinguish between *static aliasing errors* (i.e., those associated with spatial discretization) and the dynamical process that results from *combination with time stepping*. The viscous Burgers equation will serve as an example.

1.2.1. Divergence Form. We are seeking a numerical periodic solution in the interval $[0, L = 2\pi]$ to the initial and boundary value problem (IBVP), in which the nonlinear term is written in *conservation (or divergence) form*:

$$\frac{\partial u(x,t)}{\partial t} + \frac{\partial}{\partial x}\left(\frac{u^2(x,t)}{2}\right) - \nu \frac{\partial^2 u(x,t)}{\partial x^2} = 0, \tag{17a}$$

$$u(x,0) = u_0(x). \tag{17b}$$

Exact solutions are known from the Cole–Hopf transformation for any given $u_0(x)$. Applying the so-called method of lines on an N-point grid in physical space gives the semi-discrete form of (17) as a system of N ordinary differential equations (ODEs),

$$\frac{du_i^N}{dt} + \frac{1}{2} D_i^1(u^N u^N) - \nu D_i^2(u^N) = 0, \qquad i = 0, \ldots, N-1, \tag{18}$$

where $(u^N u^N)$ is the vector whose ith component is the value at the node x_i of the product $u_i^N u_i^N$.

The Fourier-collocation or pseudo-spectral approximation of (17) leads to

$$\frac{d\tilde{u}_k^N}{dt} + \frac{1}{2} j_c k \sum_{n+m=k} \tilde{u}_n^N \tilde{u}_m^N + \underbrace{\frac{1}{2} j_c k \sum_{n+m=k\pm N} \tilde{u}_n^N \tilde{u}_m^N}_{\text{aliasing}} + \nu k^2 \tilde{u}_k^N = 0, \tag{19}$$

$$k = -N/2, \ldots, N/2-1,$$

where the *static* aliasing error can be removed [2] by the 3/2-rule to get

$$\frac{d\tilde{u}_k^N}{dt} + \frac{1}{2} j_c k \sum_{n=-N/2}^{N/2-1} \tilde{u}_n^N \tilde{u}_{k-n}^N + \nu k^2 \tilde{u}_k^N = 0, \qquad k = -N/2, \ldots, N/2-1. \tag{20}$$

Now, working in physical space with (18) will produce at the node x_i, the error (16) for $du_i^N/dt - \nu D_i^2(u^N)$ before time integration, and this calculation is mimicked in spectral space by (19) provided the MWNs of the discrete differentiation operators are introduced instead of the spectral derivatives. Transforming (20) back into physical space (with introduction of MWNs) will give

$$\frac{du_i^N}{dt} + \frac{1}{2}\sum_{k=-N/2}^{N/2-1}\left(j_c k'(\omega_k)\sum_{n=-N/2}^{N/2-1}\tilde{u}_n^N\tilde{u}_{k-n}^N\right)e^{j_c\frac{2\pi}{N}ik} - \nu D_i^2(u^N) = 0. \tag{21}$$

Although the associated Fourier coefficients are dealiased, there still exists at node x_i the truncation part (II) of the global error (16).

1.2.2. Convective form. If the *convective form*

$$\frac{\partial u(x,t)}{\partial t} + u(x,t)\frac{\partial u}{\partial x}(x,t) - \nu\frac{\partial^2 u(x,t)}{\partial x^2} = 0 \tag{22}$$

is used instead of (17), the method of lines in physical space will give

$$\frac{du_i^N}{dt} + u_i^N D_i^1(u^N) - \nu D_i^2(u^N) = 0, \tag{23}$$

and since the numerical value of the product $u_i^N D_i^1(u^N)$ is exact at physical grid points, no static error is introduced before time integration for $du_i^N/dt - \nu D_i^2(u^N)$. Fourier-collocation discretization of (22) reads

$$\frac{d\tilde{u}_k^N}{dt} + \sum_{n+m=k}\tilde{u}_n^N\left(j_c m\tilde{u}_m^N\right) + \sum_{n+m=k\pm N}\tilde{u}_n^N\left(j_c m\tilde{u}_m^N\right) + \nu k^2\tilde{u}_k^N = 0, \tag{24}$$

or alternatively

$$\frac{d\tilde{u}_k^N}{dt} + \frac{1}{2}j_c k\sum_{n+m=k}\tilde{u}_n^N\tilde{u}_m^N + \underbrace{\frac{1}{2}j_c(k\pm N)\sum_{n+m=k\pm N}\tilde{u}_n^N\tilde{u}_m^N}_{\text{aliasing}} + \nu k^2\tilde{u}_k^N = 0, \tag{25}$$

$$n, m, k = -N/2, \ldots, N/2-1,$$

which differs from (19) in the aliasing term (which is of opposite sign, making the skew-symmetric form popular in pseudo-spectral methods). Introduction of the MWN in (25) will mimic (23); but if dealiasing is performed, that is,

$$\frac{d\tilde{u}_k^N}{dt} + \sum_{n+m=k}\tilde{u}_n^N\left(j_c m'(m)\tilde{u}_m^N\right) + \nu k'^2(k)\tilde{u}_k^N = 0, \tag{26}$$

transforming (26) back into physical space does not correspond to any physical space finite difference implementation.

1.2.3. Answer to item (iii). From Sections 1.2.1 and 1.2.2, the numerical errors produced either by the divergence or the convective forms of nonlinear terms in physical space can be mimicked and thus analyzed by pseudo-spectral codes with MWNs, but without dealiasing. Dealiasing in pseudo-spectral calculations is of no help to the analysis of numerical errors introduced in physical space calculations. Physical space errors should rather refer to a calculation involving *only* MWN static errors and optimum conservation properties; that is, due to (11)–(13),

$$\frac{du_i^N}{dt} + \frac{1}{2}\sum_{k=-N}^{N-1} j_c k'(\omega_k)\tilde{w}_k^{2N} e^{j_c \frac{2\pi}{2N} 2ik} - \nu D_i^2(u^N) = 0, \qquad i = 0, \ldots, N-1. \tag{27}$$

1.3. *Toward the Lowest Error in Physical Space*

The divergence form is very popular in physical space for its conservative properties [14, 18], mainly in compressible flows, but has the drawback of introducing the high level of error previously described in the case of marginal resolution. So, numerical techniques designed for reducing these errors may be useful for people working with this form. Although dealiasing in spectral space is a well-known technique, there is at present time no equivalence in physical space to get (27) from (18). In this section, two methods will be examined: filtering on finer grids and a midpoint interpolation technique.

1.3.1. Filtering. Quite recently, Ghosal [4] proposed the following technique to reduce numerical errors. This technique is designed to damp the modes poorly resolved by the derivation scheme, i.e., the modes such that $k'(\omega_k)$ is, say, over 0.1% error away from k. If we are only interested in (or if the solution is physically limited to) modes lower than or equal to $k_s = \pi N/L = N/2$, then, we can use a finer M-point grid with higher numerical cutoff $k_c = M/2$ and apply a low-pass "sharp Fourier-like" filter to eliminate modes between k_s and k_c which are generated by nonlinear interactions. Ghosal concluded that if $k_s < 2k_c/3$, from the 2/3 rule, no aliasing errors could occur. This conclusion is also mentioned by Lund [9] in the context of explicit and test filtering in dynamic LES of isotropic turbulence with a pseudo-spectral code.

Applied to the Burgers equation, the filtering technique reads

$$\frac{du_i^M}{dt} + \frac{1}{2} D_i^1(F(u^M u^M)) - \nu D_i^2(u^M) = 0, \qquad i = 0, \ldots, M-1, \tag{28}$$

where $F(\cdot)$ stands for the filtering operator. Consider a true sharp Fourier cutoff at mode k_s. Filtered coefficients of u are

$$\widehat{\tilde{u}}_k^M = \hat{F}(k)\tilde{u}_k^M = \begin{cases} \tilde{u}_k^M & \text{if } |k| \le k_s, \\ 0 & \text{otherwise.} \end{cases} \tag{29}$$

Then we have

$$I_M F(u^M u^M)(x_i) = \sum_{k=-M/2}^{M/2-1} \hat{F}(k)\tilde{w}_k^M e^{j_c \frac{2\pi}{M} ik} = \sum_{k=-k_s}^{k_s} \tilde{w}_k^M e^{j_c \frac{2\pi}{M} ik}, \qquad i = 0, \ldots, M-1. \tag{30}$$

Let us consider a single mode $k = 1$ initial condition (17b). Advancing (28) in time will produce by nonlinear interactions higher modes until the filter is actually active, and at any time the wave number content of the numerical solution will be limited to k_s. So solving (28) in physical space is equivalent to solving in spectral space

$$\frac{d\tilde{u}_k^M}{dt} + \frac{1}{2} j_c k'(\omega_k) \hat{F}(k) \left(\sum_{n=-k_s}^{k_s} \tilde{u}_n^M \tilde{u}_{k-n}^M + \sum_{n=-k_s}^{k_s} \tilde{u}_n^M \tilde{u}_{k-n\pm M}^M \right) + \nu k''(\omega_k) \tilde{u}_k^M = 0, \quad (31)$$
$$k = -M/2, \ldots, M/2 - 1, \qquad \tilde{u}_k^M = 0 \qquad \text{if } N/2 < |k| \le M/2,$$

and the aliasing error will be zero up to $|k| = k_s$ if $k - n \pm M = \pm k_s$, that is,

$$k_s = M/3 = \frac{2}{3}(M/2 = k_c). \quad (32)$$

This is the 2/3 truncation rule for static dealiasing in spectral space. Rewriting (28) in the form

$$\frac{du_i^M}{dt} + \frac{1}{2} \sum_{k=-M/2}^{M/2-1} \left(j_c k'(\omega_k) \hat{F}(k) \sum_{n=-k_s}^{k_s} \tilde{u}_n^M \tilde{u}_{k-n}^M \right) e^{j_c \frac{2\pi}{M} ik} - \nu D_i^2(u^M) = 0, \quad (33)$$
$$i = 0, \ldots, M-1, \qquad k_s \le M/3,$$

we can see that the convolution sum produces possible modes ranging from $-2k_s$ to $2k_s$ and that the sharp Fourier filter truncates it to $\pm k_s$, which is below the grid cutoff. The static derivation error at the nodes x_i for the nonlinear term then becomes

$$D_i^1(e) = -\sum_{k=-2k_s}^{-k_s-1} \left(j_c k'(\omega_k) \hat{F}(k) \sum_{n=-k_s}^{k_s} \tilde{u}_n^M \tilde{u}_{k-n}^M \right) e^{j_c k x_i}$$
$$- \sum_{k=k_s+1}^{2k_s} \left(j_c k'(\omega_k) \hat{F}(k) \sum_{n=-k_s}^{k_s} \tilde{u}_n^M \tilde{u}_{k-n}^M \right) e^{j_c k x_i}, \quad (34)$$

which is part (II) of (16) combined with the transfer function of the filter in physical space. Since it is very difficult to design sharp filters in physical space, this 2/3 filtering technique may introduce some new kind of error due to the "nonsharpness" of the filter. The spectral-like filters designed by Lele [7] are good candidates because of their easy tuning and high accuracy. Pentadiagonal filters are built in the following way:

$$\beta\left(\hat{u}_{i+2}^N + \hat{u}_{i-2}^N\right) + \alpha\left(\hat{u}_{i+1}^N + \hat{u}_{i-1}^N\right) + \hat{u}_i^N$$
$$= a u_i^N + \frac{b}{2}\left(u_{i+1}^N + u_{i-1}^N\right) + \frac{c}{2}\left(u_{i+2}^N + u_{i-2}^N\right) + \frac{d}{2}\left(u_{i+3}^N + u_{i-3}^N\right). \quad (35)$$

And the associated transfer function is

$$\hat{F}(\omega_k) = \frac{a + b\cos(\omega_k) + c\cos(2\omega_k) + d\cos(3\omega_k)}{1 + 2\alpha\cos(\omega_k) + 2\beta\cos(2\omega_k)}. \quad (36)$$

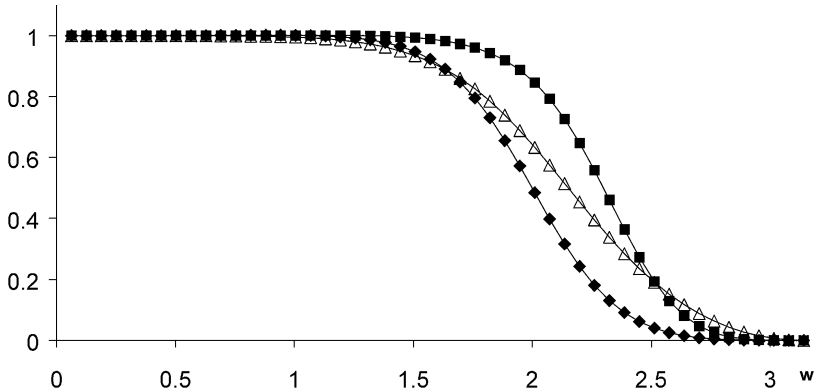

FIG. 3. Filtering transfer function (Eq. (36)). —◆—, filter 1, fourth order: 1.50/0.95–2.00/0.50; —■—, filter 2, fourth order: 1.80/0.95–2.30/0.50; —△—, filter 3, sixth order: 1.80/0.80–2.50/0.20.

Two parameters are free for tuning the scheme (by imposing the value of (36) at two given reduced wave numbers) if a sixth order is imposed, or a fourth order with the additional constraint $d^2T/d\omega^2(\pi) = 0$, the condition $dT/d\omega(\pi) = 0$ being automatically verified. The transfer functions of three different filters which are as sharp as possible within a $2/3$ cutoff are plotted on Fig. 3. In Fig. 4 is plotted the combination of the sixth-order filtering transfer function 3 and the MWN of the derivation scheme (6). The loss in resolving efficiency at $\omega \approx 2$ due to the physically designed "not-so-sharp" filter is apparent.

1.3.2. Interpolation. Since from (15), spectral aliasing is equivalent to truncation for convolution sums when transformed back into physical space, we are led to deal with entire convolution sums to recover (27) in physical space. The problem is obviously the numerical estimation of $I_{2N}w(\bar{x}_j) = u_j^{2N}v_j^{2N}$, that is, the interpolation of u and v at the nodes of a double density physical grid and the associated numerical error. This can be achieved using a compact finite difference midpoint interpolation scheme such as those designed by Lele

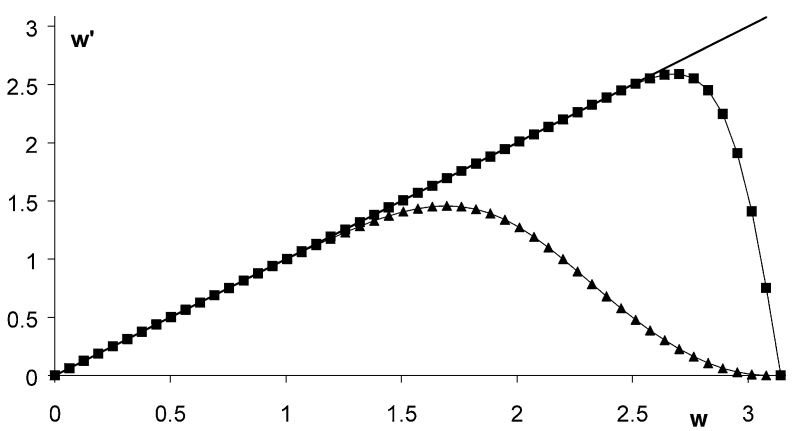

FIG. 4. MWN for derivative/filtering. —, exact; —■—, derivative only (7); —▲—, derivative + filtering (7)*(36).

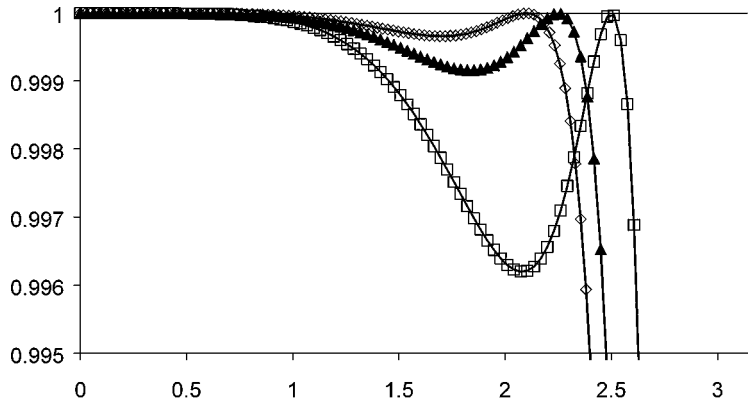

FIG. 5. Interpolation transfer function (Eq. (38)). —, Exact; -◇-, $W = 2.10$; -▲-, $W = 2.25$; -□-, $W = 2.50$.

[7], with spectral-like accuracy. The scheme reads

$$\begin{aligned}&\beta\left(u_{i+2}^N + u_{i-2}^N\right) + \alpha\left(u_{i+1}^N + u_{i-1}^N\right) + u_i^N \\ &\quad = \frac{c}{2}\left(u_{i+5/2}^N + u_{i-5/2}^N\right) + \frac{b}{2}\left(u_{i+3/2}^N + u_{i-3/2}^N\right) + \frac{a}{2}\left(u_{i+1/2}^N + u_{i-1/2}^N\right)\end{aligned} \tag{37}$$

and may be tuned for order and transfer function. Designed that way, it gives readily the discrete values at nodes x_i from the values at midpoints $x_{i+1/2} = (x_i + x_{i+1})/2$. It is only a matter of translation of indices to get midpoint values from solid points values. The transfer function associated with scheme (37) is, at mode k,

$$T(\omega_k) = \frac{a\cos(\omega_k/2) + b\cos(3\omega_k/2) + c\cos(5\omega_k/2)}{1 + 2\alpha\cos(\omega_k) + 2\beta\cos(2\omega_k)} \tag{38}$$

and is plotted in Fig. 5 for a sixth-order scheme such that $T = 1$ and $dT/d\omega_k = 0$ for $\omega_k = 2.10$, 2.25, and 2.50.

The set of discrete values $\bar{u}^{2N}$ is now built by gathering solid points u^N and midpoint interpolated $\bar{u}^N$ values, i.e.,

$$\begin{cases} \bar{u}_{2i}^{2N} = u_i^N, & i = 0, \ldots, N, \\ \bar{u}_{2i+1}^{2N} = \bar{u}_{i+1}^N, & i = 0, \ldots, N-1. \end{cases} \tag{39}$$

Nevertheless, the coefficients $\tilde{\bar{u}}_n^{2N}$ of $I_{2N}\bar{u}$ are altered (compared to those $\tilde{u}_n^N$ of $I_N u$) since interpolation is not exact. From

$$\bar{u}_i^N \approx u_{i-1/2}^N = \sum_{n=-N/2}^{N/2-1} T(\omega_n)\tilde{u}_n^N e^{j_c \frac{2\pi}{N}(i-1/2)n}, \tag{40}$$

we have

$$\tilde{\bar{u}}_n^N = T(\omega_n)\tilde{u}_n^N e^{-j_c \frac{\pi}{N} n}. \tag{41}$$

Hence,

$$\tilde{u}_n^{2N} = \frac{1}{2N} \sum_{m=-N/2}^{N/2-1} \tilde{u}_m^N \left(1 + T(\omega_m) e^{j_c \frac{\pi}{N}(m-n)}\right) \sum_{i=0}^{N-1} e^{j_c \frac{2\pi}{N} i(m-n)}. \tag{42}$$

The last sum (over i) in (42) is N if $m - n = rN$; it is 0 otherwise. The possible values for r are -1 and 0 if $m \leq 0$, or 0 and 1 if $m > 0$. So, each mode of u^N will produce two modes for $\overline{u}^{2N}$:

$$\tilde{u}_{n=m}^{2N} = \frac{1}{2}\tilde{u}_m^N(1 + T(\omega_m)), \tag{43a}$$

$$\tilde{u}_{n=m-\mathrm{sign}(m)N}^{2N} = \frac{1}{2}\tilde{u}_m^N(1 - T(\omega_m)). \tag{43b}$$

That is, $\tilde{w}_k^{2N}$ may be expressed as

$$\tilde{w}_k^{2N} = \sum_{n+m=k} \frac{1}{2}\tilde{u}_n^N \tilde{v}_m^N (1 + T(\omega_n)T(\omega_m)) + \sum_{n+m=k\pm N} \frac{1}{2}\tilde{u}_n^N \tilde{v}_m^N (1 - T(\omega_n)T(\omega_m)), \tag{44}$$

$$n, m = -N/2, \ldots, N/2 - 1 \qquad k = -N, \ldots, N - 1.$$

Notice that (43) and (44) are consistent with exact interpolation, i.e., with the case $T(\omega) = 1$, and that the error introduced by interpolation (the difference between (12) and (44)) is due to both the transfer function of the interpolation scheme and the associated "parasitic" modes (43b). This error reads

$$\sum_{n+m=k} \frac{1}{2}\tilde{u}_n^N \tilde{v}_m^N (1 - T(\omega_n)T(\omega_m)) - \sum_{n+m=k\pm N} \frac{1}{2}\tilde{u}_n^N \tilde{v}_m^N (1 - T(\omega_n)T(\omega_m)). \tag{45}$$

Figure 6 represents the error (45) at mode $k = n + m$ of the convolution computed from single mode real-valued functions u and v, with $|\tilde{u}_n^N| = |\tilde{v}_m^N| = 1$; $n, m \geq 0$. The aliasing error is displayed in Fig. 7. The improvement is evident.

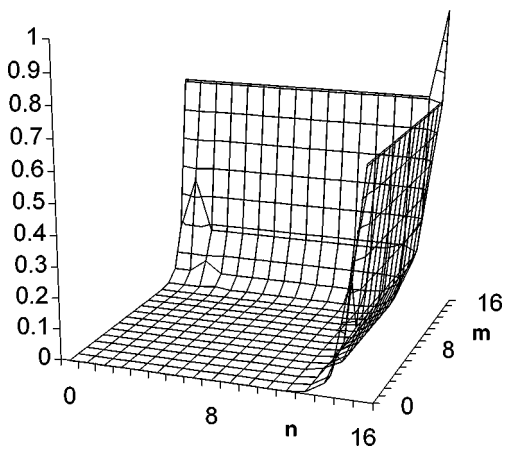

FIG. 6. Interpolation error for mode $n + m$ (Eq. (45)).

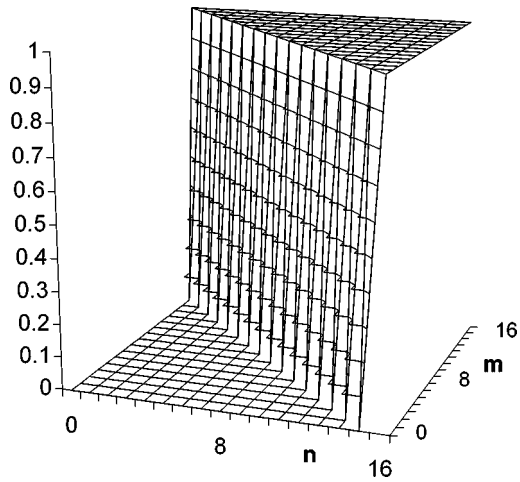

FIG. 7. Aliasing error for mode $n+m$ (second sum in Eq. (10)).

Derivation of $\bar{w}^{2N}$ on the $2N$-point grid, retaining only the result at solid points $x_i = \bar{x}_{2i}$, will now give

$$I_{2N}D^1(\bar{w}^{2N})(\bar{x}_{2i}) = D^1_{2i}(\bar{w}^{2N}) = \sum_{k=-N}^{N-1} j_c k'(\omega_k)\tilde{\bar{w}}^{2N}_k e^{j_c \frac{2\pi}{2N} 2ik}. \tag{46}$$

If we assume $v = u$ and consider modes $k = n+m$, $|n-m|$ and their opposites, the MWN of scheme (46) is

$$\bar{k}'\left(\omega_{\substack{k=n+m \\ k=|n-m|}}\right) = \frac{1}{2}k'(\omega_k)(1 + T(\omega_n)T(\omega_m)), \tag{47}$$

and for the parasitic modes

$$\bar{k}'\left(\omega_{\substack{k=-(n+m)+N \\ k=-|n-m|+N}}\right) = \frac{1}{2}k'(\omega_k)\,(1 - T(\omega_n)T(\omega_m))\,. \tag{48}$$

Reduced wave numbers (47) and (48) are plotted in Fig. 8 for $n = m$. The loss in resolving efficiency due to interpolation is negligible compared to that in Fig. 4, and parasitic modes that appear in the energetic range of the spectrum are kept at very low level due to the spectral-like accuracy of the schemes.

So, applied to the viscous Burgers equation, the interpolation technique reads

$$\frac{du_i^N}{dt} + \frac{1}{2}\sum_{k=-N}^{N-1} j_c k'(\omega_k)\tilde{\bar{w}}^{2N}_k e^{j_c \frac{2\pi}{2N} 2ik} - \nu D_i^2(u^N) = 0, \qquad i = 0, \ldots, N-1. \tag{49}$$

1.3.3. Filtering versus interpolation. We have chosen here an example specially designed to enhance the error (34) in the filtering technique for illustration.

Applied to the convolution $w(x) = u^2(x)$ for $u(x) = \sin k_1 x + \sin k_2 x$, filtering Eq. (30) with $N = 32$; $M = 48$ in the non-N-aliased $k_1 = 6$; $k_2 = 8$ and N-aliased $k_1 = 10$; $k_2 = 13$ cases gives the results plotted respectively on Figs. 9 and 10. In the non-aliased case, the

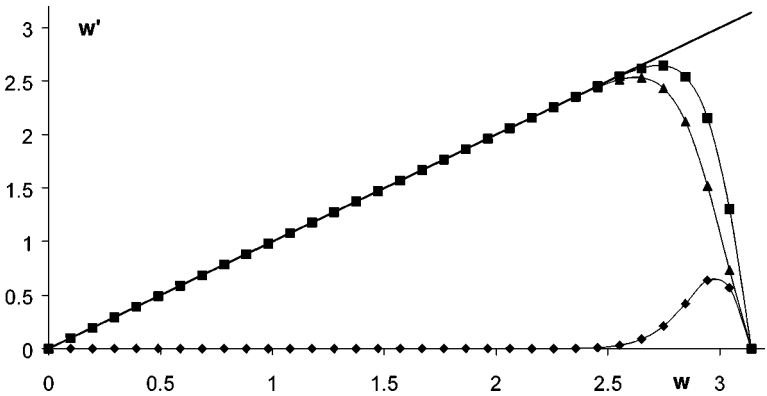

FIG. 8. MWN derivation and interpolation. —, Exact; –■–, derivation only (7); –▲–, derivative + Interpolation (47); –◆–, parasitic modes (48).

effect of the "nonsharpness" of the filter is clearly pointed out. In the aliased (dealiased by filtering) case, the strong damping of modes 20 and 23, which could stay on the 48-point grid, and of mode 26 (aliasing the mode 22) leaves only mode 3 and leads to large errors at grid points for the filtered quadratic products. On the other hand, the interpolation technique does not affect the solid points' values.

Comparison is shown in Fig. 11 for the derivative of filtered and interpolated convolution in the aliased case. The result is clear. Nevertheless, in real calculations (e.g., as in Section 1.4), the filtering technique is expected to do much better.

One can estimate roughly the extra cost of both methods (Eqs. (28) and (49)) compared to the standard one (Eq. (18)): The structure of the matrix formulation of scheme (6) leads to a global $O(N)$ cost. So, first and second derivatives estimation in (18) is $2 \times O(N)$.

The spatial discretization for Eq. (28) is $2\,O(3N/2)$ plus an extra $O(3N/2)$ for filtering, and an extra ${}^1/_2 O(N)$ for the product. So the extra cost is $3O(N)$ per time step. The CFL stability criterion imposes a $2/3$ ratio in time stepping. The interpolation requires $O(N)$ operation and the derivation requires $O(2N)$. The extra cost is then $2O(N)$ plus an extra $O(N)$ for the product; thus it is the same extra cost as for the filtering technique on the finer $3N/2$ grid, while the time stepping is unchanged.

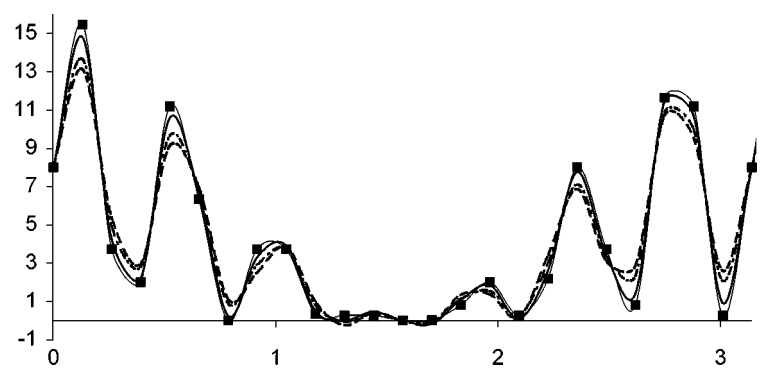

FIG. 9. Filtered convolution (Eq. (30)), for modes 6 and 8, with no aliasing. –■–, Exact; – –, filter 1; —, filter 2; – -, filter 3.

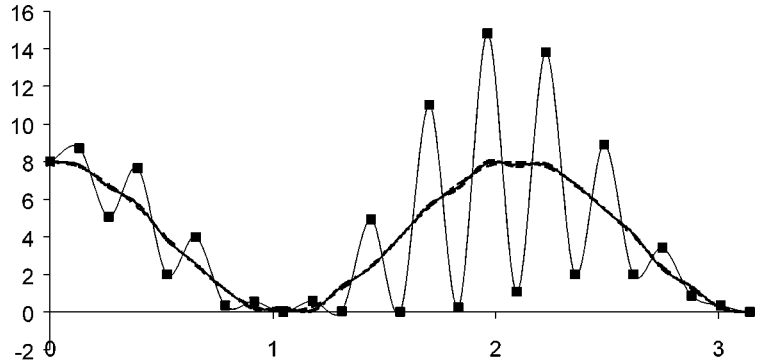

FIG. 10. Filtered convolution (Eq. (30)), for modes 10 and 13, with aliasing for modes 6, 9, and 12. –■–, Exact; – –, filter 1; —; filter 2; – -, filter 3.

Interpolation seems to be a better technique than filtering to make the divergence form nearly grid-exact and therefore equivalent to the convective form (for smooth problems) in physical space. Nevertheless, with a suitable filter, the filtering technique may be used to ensure a stable, oscillation-free numerical solution [16]. *This answers item (iv).*

1.4. *Dynamical Tests on the Burgers Equation*

The Burgers equation is solved on an $N = 128$ point grid for the initial condition $u_0 = \sin x$ on an $L = 2\pi$ domain. The time stepping is achieved with a fourth-order Runge–Kutta scheme with $\Delta t = 10^{-4}$ to push the temporal errors below the spatial ones.

1.4.1. L^2 norm of error. First, the discrete L^2 norm of error,

$$\|u^N - u_{\text{exact}}\|_{L^2}(t) = \left(\frac{1}{N} \sum_{i=0}^{N-1} \left(u_i^N(t) - u_{\text{exact}}(x_i, t) \right)^2 \right)^{1/2},$$

is evaluated in the viscous case for which an exact solution is known [19]. For a value of $\nu = 0.01$, the exact solution spectrum reaches half the grid cutoff $k = 32$ at time $t \approx 0.45$ and reaches the grid cutoff $k_c = 64$ at time $t \approx 0.70$, with an amplitude $|\tilde{u}_{\text{exact}}(k)| \approx 10^{-10}$. No aliasing error can occur before $t \approx 0.45$. Equations (18), (23), (28), and (49) are

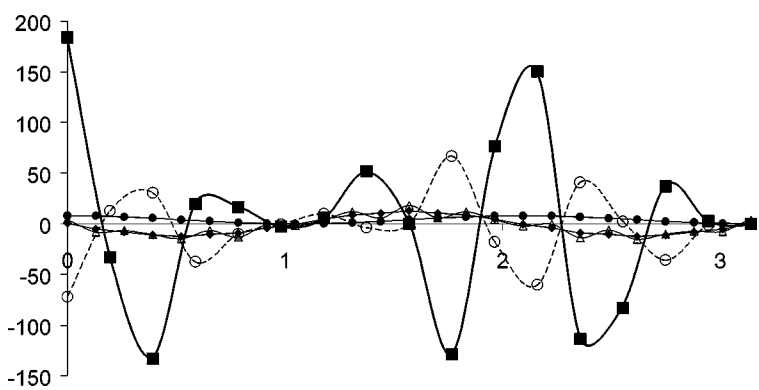

FIG. 11. Derivative of convolution, for modes 10 and 13, with aliasing for modes 6, 9, and 12. ■, Exact; —, interpolation; –⊖–, aliased; –◆–, filter 1; –●–, filter 2; –△–, filter 3.

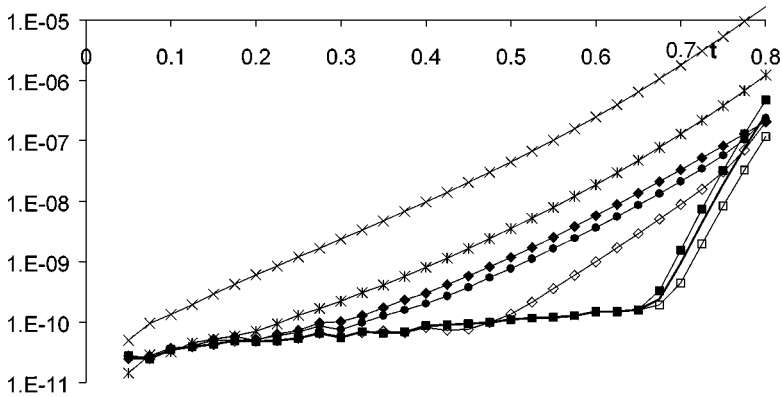

FIG. 12. L^2 norm of error for viscous Burgers equation in early stages. —◆—, Eq. (18); —■—, Eq. (19); —, Eq. (20); —◇—, Eq. (23); —⊟—, Eq. (24); —✳—, Eq. (28); —×—, Eq. (28) with $M = N$; —●—, Eq. (49).

solved in physical space with finite difference scheme (6). Equations (19), (20), and (24) are solved in spectral space with a pseudo-spectral code, dealiased (Eq. 20) or not (Eqs. (19) and (24)).

In the early stages of the computation (Fig. 12), since only discretization errors are involved, spectral simulations (19), (20), and (24) give the exact solution at machine precision, and the MWN effect in the finite difference calculations appears first for the divergence form (18) which has to deal with twice the wave number content felt in the convective form (23). The transfer function of the filtering scheme combined with the MWV of the first derivative gives a higher numerical error, although the global resolution in (28) is $3N/2$. The results of (28) for $M = 126 \approx N$ grid points are also displayed. The interpolation technique (49) provides a good balance between the loss in precision due to its transfer function and the increase in resolving efficiency of the derivative scheme.

At $t \approx 0.45$, the time stepping begins to act on aliased nonlinearities due to marginal resolution and the error for the convective form (23) begins to grow. The aliasing errors in the spectral calculations (19) and (24) are harmless for this problem until $t \approx 0.70$ when the solution itself begins to be under-resolved.

Once under-resolution is reached (Fig. 13), the better job is done by (28) since it is one-half more resolved than other calculations. Aliasing errors in spectral calculations are dominant for the divergence form (19), but have a stabilizing effect (opposite to the Gibbs phenomenon in (20)) for the convective form (24). MWNs in finite difference calculations damp aliasing errors at high wave numbers and so (18) does better than (19), and (23) does a little worse than (24). The interpolation technique (49) gives nearly the same level of error as (23), though it is slightly increased by the transfer function of the interpolation scheme. The solution at time $t = 1.6$, when errors are maximum, is shown on Fig. 14 for (18), (23), (28), and (49).

1.4.2. Energy conservation. To check the energy conservation of the discrete methods, the viscosity is set to zero. No analytical solution exists, but the energy must be conserved by nonlinear terms in this periodic problem. The energy in the discrete solution is

$$E(t) = \frac{1}{N} \sum_{i=0}^{N-1} u_i^N(t)^2.$$

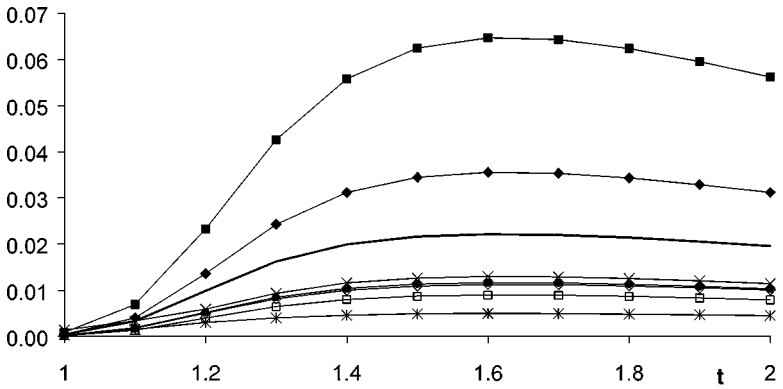

FIG. 13. L^2 norm of error for viscous Burgers equation after under-resolution is mached. —◆—, Eq. (18); —■—, Eq. (19); —, Eq. (20); —◇—, Eq. (23); —□—, Eq. (24); —✳—, Eq. (28); —×—, Eq. (28) with $M = N$; —●—, Eq. (49).

Theoretically, the fully discrete approximation must use a symmetric time scheme to satisfy the conservation properties of the semi-discrete one [2]. Here, the very small time step in the nonsymmetric Runge–Kutta scheme makes the semi- and fully discrete approximations numerically equivalent at machine precision. This is checked for the spectral dealiased calculation (20).

Figure 15 displays the evolution $E(t) - E(0)$. The divergence form is unstable for both aliased spectral (19) and finite difference (18) calculations, as already mentioned by Kravchenko and Moin [6]. The convective form does not conserve energy and the interpolation technique (49) is once again very close to (23). The filtering technique (28) is the most conservative on the finer grid but rather dissipative on the standard grid. *This answers item (v).*

1.5. *Conclusions of the First Part*

In the first part of this study, we have pointed out that the divergence form of nonlinear PDEs advanced in time in physical space with spectral-like schemes may produce large

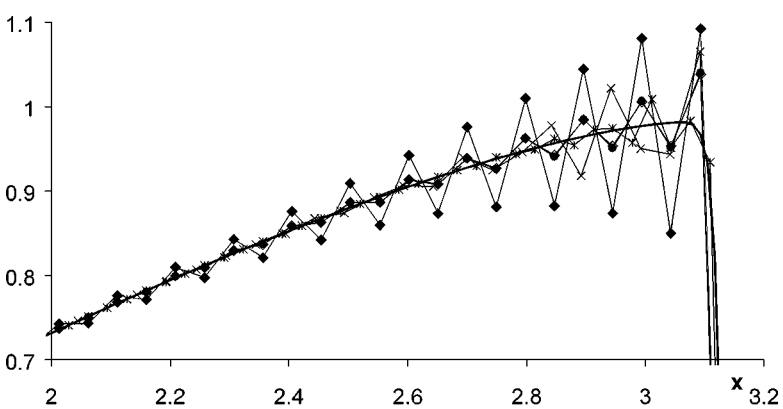

FIG. 14. Solution of viscous Burgers equation at $t = 1.6$. —, Exact; —◆—, Eq. (18); —◇—, Eq. (23); —●—, Eq. (49); —✳—, Eq. (28); —×—, Eq. (28) with M = N.

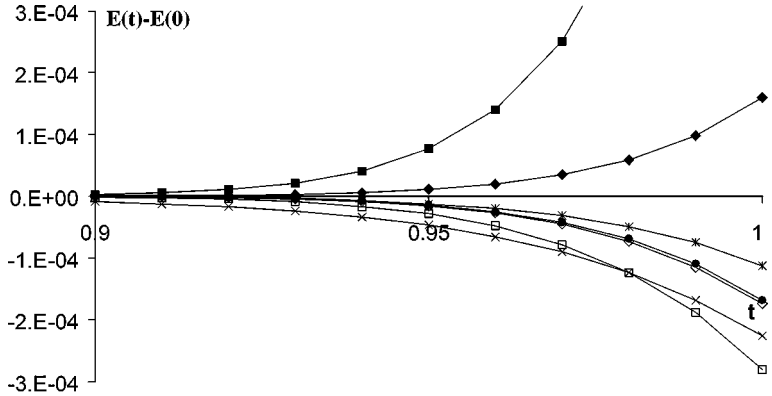

FIG. 15. Evolution of energy for inviscid Burgers equation. —◆—, Eq. (18); —■—, Eq. (19); —, Eq. (20); —◇—, Eq. (23); —⊟—, Eq. (24); —✳—, Eq. (28); —✕—, Eq. (28.) with M = N; —●—, Eq. (49).

errors due to the combination of static aliasing and time stepping. The convective form, on the other hand, has better long-time behavior. These errors may be mimicked using aliased pseudo-spectral codes with MWNs of the scheme, but spectral dealiasing doesnot provide any straightforward information for physical space implementation of finite difference schemes. This is the key point for the second part of this paper. The divergence form associated with a midpoint interpolation technique is nearly equivalent to the convective form, which is grid-exact before time stepping. Using a finer grid and applying a filtering operation is a suitable method for smoothing the solution and hence improving the global stability of the numerical method, but it is more expensive due to refinement in time stepping required by stability conditions (e.g., CFL).

2. NUMERICAL TESTS FOR FILTERED NAVIER–STOKES EQUATIONS

We turn now to the LES of the Navier–Stokes equations to compare the relative magnitude of aliasing and truncation errors with the subgrid scale term for various forms of the nonlinearities which will be detailed in Section 2.2, and for two discretization schemes:

- DF2: second-order central finite difference scheme and
- SL4: fourth-order compact scheme (6) with 80.0% of resolving efficiency at 0.1% error.

The reference pseudo-spectral discretization schemes will be referred to as

- SP: Fourier-collocation (aliased) and
- SPDA: Fourier-collocation dealiased.

This numerical experiment is performed on self-decaying isotropic homogeneous turbulence with a pseudo-spectral code at resolution 48^3.

2.1. *Static Aliasing in 3D*

In three dimensions of space, pseudo-spectral evaluation of convolution sums produces more complex aliasing errors. Considering a cubical domain of size $(L = 2\pi)^3$ aligned

with the orthonormal basis $(\mathbf{e}_1, \mathbf{e}_2, \mathbf{e}_3)$, the discrete representation of a scalar field $u(\mathbf{x})$ is

$$I_N^3 u(\mathbf{x}) = u^N_{i_1 i_2 i_3} = \sum_{\mathbf{k}} \tilde{u}^N_{k_1 k_2 k_3} e^{j_c \mathbf{k}\cdot\mathbf{x}} \tag{50a}$$

$$\tilde{u}^N_{k_1 k_2 k_3} = \frac{1}{N^3} \sum_{\mathbf{x}} u^N_{i_1 i_2 i_3} e^{-j_c \mathbf{k}\cdot\mathbf{x}}, \tag{50b}$$

where

$$\mathbf{x} = x_{1 i_1}\mathbf{e}_1 + x_{2 i_2}\mathbf{e}_2 + x_{3 i_3}\mathbf{e}_3,$$
$$x_{\alpha i_\alpha} = \frac{i_\alpha L}{N}, \qquad i_\alpha = 0, \ldots, N-1, \qquad \alpha = 1, 2, 3$$

and

$$\mathbf{k} = k_{1 n_1}\mathbf{e}_1 + k_{2 n_2}\mathbf{e}_2 + k_{3 n_3}\mathbf{e}_3,$$
$$k_{\alpha n_\alpha} = n_\alpha \frac{2\pi}{L} = n_\alpha, \qquad n_\alpha = -N/2, \ldots, N/2 - 1, \qquad \alpha = 1, 2, 3$$

are discrete grid points and discrete wave vectors respectively. The discrete representation of the product $w(\mathbf{x}) = u(\mathbf{x})v(\mathbf{x})$ is then

$$I_N^3 w(\mathbf{x}) = w^N_{i_1 i_2 i_3} = \sum_{\mathbf{k}} \tilde{w}^N_{k_1 k_2 k_3} e^{j_c \mathbf{k}\cdot\mathbf{x}}, \tag{51a}$$

$$\tilde{w}^N_{k_1 k_2 k_3} = \frac{1}{N^3} \sum_{\mathbf{x}} u^N_{i_1 i_2 i_3} v^N_{i_1 i_2 i_3} e^{-j_c \mathbf{k}\cdot\mathbf{x}}, \tag{51b}$$

with

$$\tilde{w}^N_{k_1 k_2 k_3} = \sum_{\mathbf{p}+\mathbf{q}=\mathbf{k}} \tilde{u}^N_{p_1 p_2 p_3} \tilde{v}^N_{q_1 q_2 q_3} + \tilde{\mathrm{S}} + \tilde{\mathrm{D}} + \tilde{\mathrm{T}}, \tag{52}$$

simple aliasing
$$\tilde{\mathrm{S}} = \sum_{\alpha=1}^{3} \left(\sum_{\mathbf{p}+\mathbf{q}=\mathbf{k}\pm N\mathbf{e}_\alpha} \tilde{u}^N_{p_1 p_2 p_3} \tilde{v}^N_{q_1 q_2 q_3} \right), \tag{53a}$$

double aliasing
$$\tilde{\mathrm{D}} = \sum_{\alpha=1}^{3} \left(\sum_{\mathbf{p}+\mathbf{q}=\mathbf{k}\pm N(\mathbf{e}_1+\mathbf{e}_2+\mathbf{e}_3)\wedge\mathbf{e}_\alpha} \tilde{u}^N_{p_1 p_2 p_3} \tilde{v}^N_{q_1 q_2 q_3} \right), \tag{53b}$$

triple aliasing
$$\tilde{\mathrm{T}} = \sum_{\mathbf{p}+\mathbf{q}=\mathbf{k}\pm N(\mathbf{e}_1+\mathbf{e}_2+\mathbf{e}_3)} \tilde{u}^N_{p_1 p_2 p_3} \tilde{v}^N_{q_1 q_2 q_3}. \tag{53c}$$

Dealiasing techniques developed in one dimension of space are directly applicable to (52) [2].

2.2. *Navier–Stokes Equations*

Global quality of numerical simulation of Navier–Stokes equations (DNS and mostly LES) depends on the dynamical behavior of truncation and aliasing errors introduced in

the discretization of the nonlinear convection term N_i. For an incompressible fluid, using Einstein's convention,

$$u_{i,i} = 0, \tag{54}$$

$$\frac{\partial u_i}{\partial t} + N_i = -\frac{1}{\rho} p_{,i} + \nu u_{i,jj}. \tag{55}$$

N_i may be written in various forms that are analytically but not numerically equivalent:

$$N_i^1 = (u_i u_j)_{,j} \qquad \text{(divergence form)}, \tag{56a}$$

$$N_i^2 = u_i u_{j,j} + u_j u_{i,j} \qquad \text{(convective form)}, \tag{56b}$$

$$N_i^3 = \frac{1}{2}\left(N_i^1 + N_i^2\right) \qquad \text{(skew-symmetric form)}, \tag{56c}$$

$$N_i^{41} = \varepsilon_{ijk}(\omega_k u_j) + \frac{1}{2}(u_j u_j)_{,i} \qquad \text{(rotational form 1)}, \tag{56d}$$

$$N_i^{42} = \varepsilon_{ijk}(\omega_k u_j) + u_{i,j} u_j \qquad \text{(rotational form 2)}, \tag{56e}$$

$$\omega_k = \varepsilon_{klm} u_{m,l}.$$

For pseudo-spectral discretization, only aliasing errors differ from one form to the other, but working with finite difference schemes, either in physical space or in spectral space with the MWN, will produce various interactions of truncation and aliasing errors due to the nonlinearity of the MWN. The Fourier coefficients associated with (56), where the prime symbol stands for finite difference derivatives, are

$$\tilde{N}_i'^1(\mathbf{k}) = j_c k_j'\left(\omega_{k_j}\right) \sum_{\mathbf{p}+\mathbf{q}=\mathbf{k}} \tilde{u}_i(\mathbf{p})\tilde{u}_j(\mathbf{q}) + \tilde{\mathrm{S}}_1 + \tilde{\mathrm{D}}_1 + \tilde{\mathrm{T}}_1, \tag{57a}$$

$$\tilde{N}_i'^2(\mathbf{k}) = j_c \sum_{\mathbf{p}+\mathbf{q}=\mathbf{k}} \left(p_j'\left(\omega_{p_j}\right) + q_j'\left(\omega_{q_j}\right)\right)\tilde{u}_i(\mathbf{p})\tilde{u}_j(\mathbf{q}) + \tilde{\mathrm{S}}_2 + \tilde{\mathrm{D}}_2 + \tilde{\mathrm{T}}_2, \tag{57b}$$

$$\tilde{N}_i'^3(\mathbf{k}) = \frac{1}{2}\left(\tilde{N}_i'^1(\mathbf{k}) + \tilde{N}_i'^2(\mathbf{k})\right), \tag{57c}$$

$$\begin{aligned}\tilde{N}_i'^{41}(\mathbf{k}) = {} & \varepsilon_{ijk}\varepsilon_{klm} j_c \sum_{\mathbf{p}+\mathbf{q}=\mathbf{k}} p_l'\left(\omega_{p_l}\right)\tilde{u}_m(\mathbf{p})\tilde{u}_j(\mathbf{q}) \\ & + \frac{1}{2} j_c k_i'\left(\omega_{k_i}\right) \sum_{\mathbf{p}+\mathbf{q}=\mathbf{k}} \tilde{u}_j(\mathbf{p})\tilde{\boldsymbol{u}}_j(\mathbf{q}) + \tilde{\mathrm{S}}_{41} + \tilde{\mathrm{D}}_{41} + \tilde{\mathrm{T}}_{41},\end{aligned} \tag{57d}$$

$$\begin{aligned}\tilde{N}_i'^{42}(\mathbf{k}) = {} & \varepsilon_{ijk}\varepsilon_{klm} j_c \sum_{\mathbf{p}+\mathbf{q}=\mathbf{k}} p_l'\left(\omega_{p_l}\right)\tilde{u}_m(\mathbf{p})\tilde{u}_j(\mathbf{q}) \\ & + j_c \sum_{\mathbf{p}+\mathbf{q}=\mathbf{k}} p_j'\left(\omega_{p_j}\right)\tilde{u}_i(\mathbf{p})\tilde{u}_j(\mathbf{q}) + \tilde{\mathrm{S}}_{42} + \tilde{\mathrm{D}}_{42} + \tilde{\mathrm{T}}_{42}.\end{aligned} \tag{57e}$$

In the spectral projection of (54) and (55), one has to choose one of the various forms of (57). Another choice is given between preserving a divergence-free velocity field or not, that is, ensuring the analytical equivalence and conservation properties for all forms [18]. Taking only truncation and aliasing errors into consideration ensures conservation. Starting

from the Navier–Stokes equations in spectral space

$$j_c k_i \hat{u}_i = 0, \tag{58}$$

$$\hat{u}_{i,t} + \hat{N}_i = -j_c k_i \hat{P} - \nu k^2 \hat{u}_i, \qquad P = p/\rho, \tag{59}$$

the pressure may be eliminated by taking the divergence of (59). If the MWNs are introduced only in (59), the divergence-free velocity field is achieved at machine precision and the "biased" projection tensor on the plane normal to **k** is introduced:

$$P'_{ij}(\mathbf{k}) = \delta_{ij} - \frac{k'_i k_j}{k'_l k_l}. \tag{60}$$

The differences between spectral and biased projection tensors are plotted on Fig. 16 for schemes DF2 and SL4, in the two-dimensional case. For the diagonal terms P'_{11} and P'_{22}, one can see amplification in one direction of space and damping in the other, whereas a strong asymmetry is observed for its deviatoric part P'_{12}, mostly for higher modes.

So, the system of equations to be solved numerically is

$$\tilde{u}_{i,t} = -P'_{ij} \tilde{N}'^{n}_{j} - \nu k'' \tilde{u}_i. \tag{61}$$

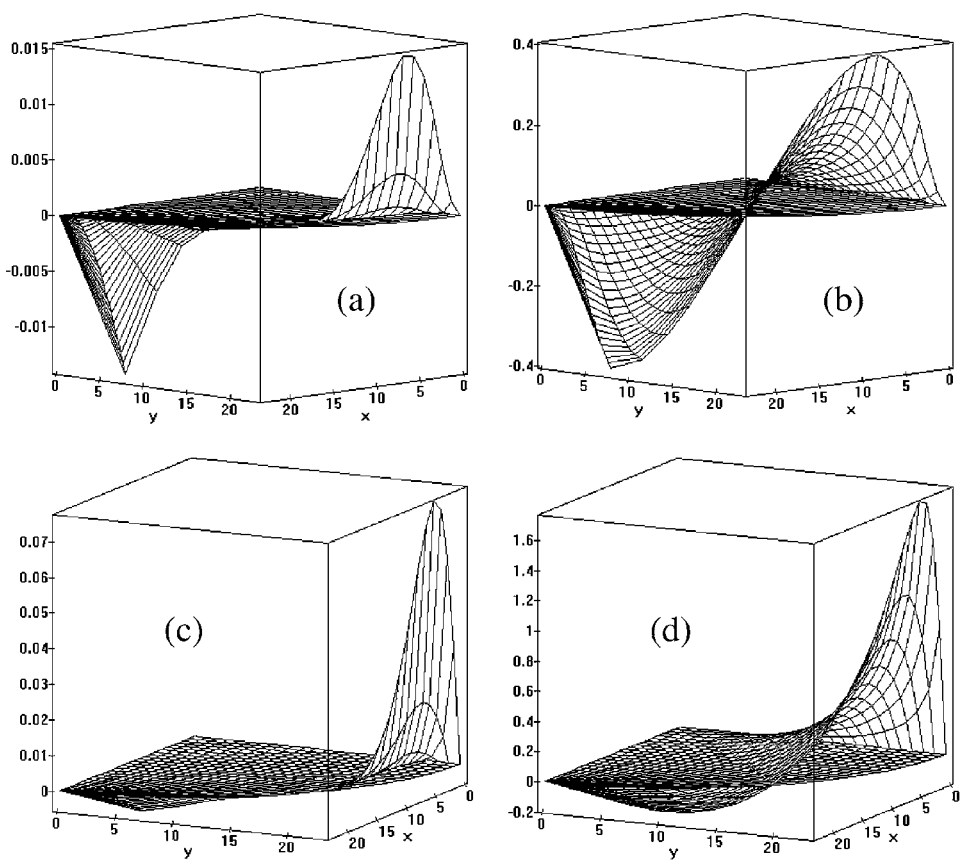

FIG. 16. Difference between spectral and biased projection tensors: (a) diagonal term SL4; (b) diagonal term DF2; (c) deviatoric term SL4; (d) deviatoric term DF2.

TABLE I
Equivalence of Nonlinear Terms by Fourier Transform

Physical space		Spectral space (all undealiased)
N^1	$\longrightarrow$	$\tilde{N}^1$
N^1 + exact interpolation	$\dashrightarrow$	
N^2	$\longrightarrow$	$\tilde{N}^2$
N^3 + exact interpolation	$\dashrightarrow$	
N^3	$\longrightarrow$	$\tilde{N}^3$
N^{41}	$\longrightarrow$	$\tilde{N}^{41}$
N^{41} + exact interpolation	$\dashrightarrow$	
N^{42}	$\longrightarrow$	$\tilde{N}^{42}$

2.3. *The Numerical Study*

2.3.1. Methodology. The first part of the numerical experiment is aimed at comparing errors of truncation and static aliasing for the various forms (56) and (57) of the nonlinear terms, applied to a filtered three-dimensional velocity field typical of an LES of isotropic homogeneous turbulence. The MWNs of schemes DF2 and SL4 are or are not introduced in a pseudo-spectral code for which dealiasing may or may not be performed.

From the results of the first part in Section 1.1 the convective N^2 and rotational N^{42} are grid-exact in physical space, although $\tilde{N}^2$ and $\tilde{N}^{42}$ are aliased in spectral space. The divergence N^1 form produces a static numerical error at grid points in physical space which is equivalent by Fourier transform to the spectral static aliasing of $\tilde{N}^1$. Skew-symmetric N^3 and rotational N^{41} produce static errors in physical space which are not related by Fourier transform to the spectral static aliasing of $\tilde{N}^3$ and $\tilde{N}^{41}$. Table I gives equivalencies by Fourier transform between physical space and aliased spectral space calculations. Solid arrows mean full equivalence, i.e., with or without MWNs, and dashed arrows mean equivalence only for exact derivatives.

The static analysis of errors for various forms is done from the error spectrum as in [4] in the following way. Suppose that $\tilde{G}_i^{\mathrm{REF}}(\mathbf{k})$ is the ith spectral component of a vector reference value and $\tilde{G}_i^{\mathrm{TEST}}(\mathbf{k})$ is its avatar obtained with a method to be characterized. The difference

$$\Delta_{\tilde{G}_i}^{\mathrm{REF-TEST}}(\mathbf{k}) = \tilde{G}_i^{\mathrm{REF}}(\mathbf{k}) - \tilde{G}_i^{\mathrm{TEST}}(\mathbf{k}) \tag{62}$$

is evaluated in spectral space at all discrete wave vectors. The error spectrum is then computed at mode k by integration on the sphere A_k of radius k and averaging over $i = 1, 2, 3$ since homogeneity and isotropy are prescribed:

$$E_{\tilde{G}}^{\mathrm{REF-TEST}}(\mathbf{k}) = \frac{1}{3}\sum_{i=1}^{3} \frac{1}{4\pi k^2} \int_{Ak} \left|\Delta_{\tilde{G}_i}^{\mathrm{REF-TEST}}(\mathbf{k})\right| dAk. \tag{63}$$

So, truncation alone, aliasing alone, and global error spectra may be obtained for the forms N^n implemented in physical space from calculations in spectral space, as explained in Table II. "SP" means spectral derivatives and "FD" means introduction of either DF2 or SL4 finite difference MWNs in derivatives, *all calculations being aliased.*

TABLE II
Procedure Technique for Error Analysis

Form	Aliasing alone	Truncation alone	Global error
N^1	$\tilde{N}^2_{\mathrm{SP}} - \tilde{N}^1_{\mathrm{SP}}$	$\tilde{N}^1_{\mathrm{SP}} - \tilde{N}^1_{\mathrm{FD}}$	$\tilde{N}^2_{\mathrm{SP}} - \tilde{N}^1_{\mathrm{FD}}$
N^2	None	$\tilde{N}^2_{\mathrm{SP}} - \tilde{N}^2_{\mathrm{FD}}$	
N^3	$\tilde{N}^2_{\mathrm{SP}} - \tilde{N}^3_{\mathrm{SP}}$	$\tilde{N}^3_{\mathrm{SP}} - \tilde{N}^3_{\mathrm{FD}}$	$\tilde{N}^2_{\mathrm{SP}} - \tilde{N}^3_{\mathrm{FD}}$
N^{41}	$\tilde{N}^{42}_{\mathrm{SP}} - \tilde{N}^{41}_{\mathrm{SP}}$	$\tilde{N}^{41}_{\mathrm{SP}} - \tilde{N}^{41}_{\mathrm{FD}}$	$\tilde{N}^{42}_{\mathrm{SP}} - \tilde{N}^{41}_{\mathrm{FD}}$
N^{42}	None	$\tilde{N}^{42}_{\mathrm{SP}} - \tilde{N}^{42}_{\mathrm{FD}}$	

2.3.2. Random velocity field generation. To perform a realistic study, a 3D Kolmogorov energy spectrum peaking at $k_I = 5$, showing an infrared region in k^4 and an inertial range in $k^{-5/3}$ reaching the cutoff at $k_c = 23$, is prescribed:

$$E(k) = \begin{cases} k^4, & 0 \le k \le k_I, \\ k^{-5/3}, & k_I \le k \le k_c. \end{cases} \tag{64}$$

Introducing the spectral vector stream function $\tilde{\boldsymbol{\Psi}}(\mathbf{k})$ such that

$$\tilde{u}_i(\mathbf{k}) = j_c k_j \varepsilon_{ijk} \tilde{\Psi}_k(\mathbf{k}) \tag{65}$$

gives

$$\tilde{u}_i \tilde{u}_i^* = (1 - \delta_{jk})(k_j k_j \tilde{\Psi}_k \tilde{\Psi}_k^* - k_j k_k \tilde{\Psi}_k \tilde{\Psi}_j^*). \tag{66}$$

On the sphere A_k of radius k, where the ensemble average operator $\langle\rangle$ is applied on the direction (or phase) of the wave vector $\mathbf{k}$ and the Dirac delta $\delta(\mathbf{0})$ vanishes using a DFT, the relation

$$\frac{E(k)}{2\pi k^2} = \langle (1 - \delta_{jk})(k_j k_j \tilde{\Psi}_k \tilde{\Psi}_k^* - k_j k_k \tilde{\Psi}_k \tilde{\Psi}_j^*) \rangle \tag{67}$$

has constant values. Then $\tilde{\Psi}(\mathbf{k})$ is built by

$$\tilde{\Psi}_i(\mathbf{k}) = \Psi(k) e^{j_c \theta_i(\mathbf{k})}, \tag{68}$$

where θ_i walks randomly in $[0, 2\pi]$.
So, on the sphere A_k

$$\frac{E(k)}{2\pi k^2} = \Psi^2(k) \left\langle (1 - \delta_{jk}) \left(k_j k_j - k_j k_k e^{j_c(\theta_k - \theta_j)} \right) \right\rangle \tag{69}$$

and

$$\Psi(k) = \left(\frac{E(k)}{4\pi k^4} \right)^{1/2}, \tag{70}$$

which gives, together with (65) and (68), the divergence-free random test field. It is checked *a posteriori* that the prescribed energy spectrum (64) is recovered (Fig. 17). Its probability density function is Gaussian.

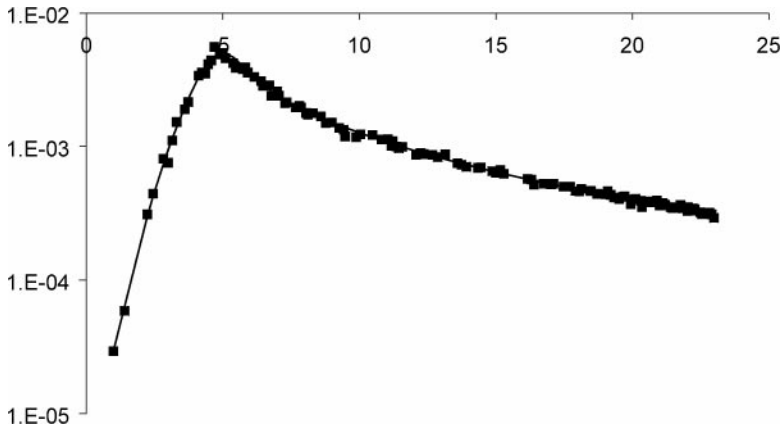

FIG. 17. Energy spectrum. ■, Recovered; —, prescribed.

2.4. *LES Formalism and Subgrid Modeling*

The eddy-viscosity assumption for the closure of filtered Navier–Stokes equations in spectral space leads to [8]

$$\left(\frac{\partial}{\partial t} + (\nu + \nu^t(k \mid k_c))k''\right)\bar{\tilde{u}}_i(\mathbf{k}, t) = t_{i,<k_c}(\mathbf{k}, t), \tag{71}$$

where

$$t_{i,<k_c}(\mathbf{k}, t) = P'_{il}(\mathbf{k})\tilde{N}^n_l(\mathbf{k}, t) \tag{72}$$

represents spectral transfer at mode $\mathbf{k}$ by triadic interactions between modes $\mathbf{p}$ and $\mathbf{q}$ such that $\mathbf{p} + \mathbf{q} = \mathbf{k}$, from the filtered velocity field and the biased projector (60). For the form N^1 (dealiased), it reads

$$t_{i,<k_c}(\mathbf{k}, t) = -j_c k'_j\left(\omega_{k_j}\right) P'_{il}(\mathbf{k}) \sum_{\substack{\mathbf{p}+\mathbf{q}=\mathbf{k} \\ |\mathbf{p}|\text{and}|\mathbf{q}|\text{and}|k| \le k_C}} \tilde{u}_l(\mathbf{p}, t)\tilde{u}_j(\mathbf{q}, t). \tag{73}$$

Subgrid scale transfers are modeled from the concept of spectral eddy viscosity of Kraichnan [5] with the dynamic model developed by Métais *et al.* [10], which allows for a k^{-m} energy spectrum at the cutoff:

$$\nu^t(k \mid k_c) = \nu^{t+}(k \mid k_c)\left(\frac{E(k_c, t)}{k_c}\right)^{1/2}. \tag{74}$$

The eddy viscosity, normalized with the value of the spectrum at the cutoff, is amended to produce a cusp near k_c where the energetic transfer is more important:

$$\nu^{t+}(k \mid k_c) = \nu^{t+\infty}\left(1 + 34.5e^{-3.03(k_c/k)}\right). \tag{75}$$

For k_c lying in the middle of a $k^{-5/3}$ Kolmogorov inertial range, the asymptotic (plateau value) of (75),

$$\nu^{t+\infty} = 0.31\, C_K^{-3/2}\frac{5-m}{m+1}(3-m)^{1/2}. \tag{76}$$

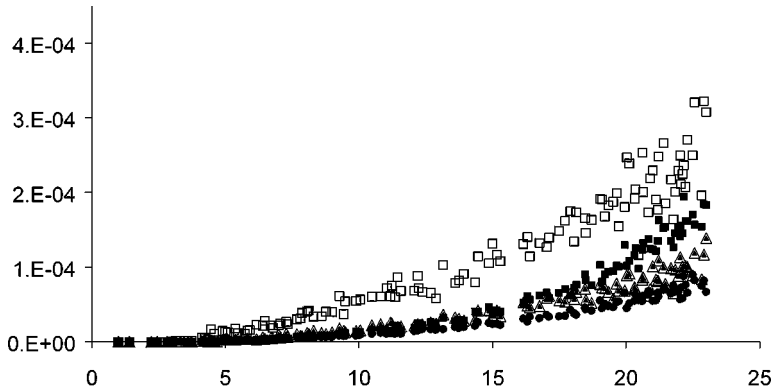

FIG. 18. Spectral aliasing. ■, N^1; ▲, N^2; ●, N^3; □, N^{41}; △, N^{42}.

recovers its eddy damped quasi-normal Markovian theory (EDQNM) predicted value

$$\nu^{t+\infty} = 0.441\ C_K^{-3/2} \approx 0.267.$$

Note that in (71), the product $\nu^t k''$ allows for a straightforward analysis of the interactions of the subgrid scale model and the second order derivation scheme (Section 2.5.3).

2.5. *Term by Term Analysis*

2.5.1. Convective terms N^n. Figures 18 to 29 show aliasing, truncation, and global error spectra with the same scaling for a better visual comparison. In spectral space, all forms produce aliasing errors (Fig. 18). Spectral aliasing errors spectra have been calculated from the difference between spectral aliased and dealiased calculations. As expected from Eqs. (56a), (56c), and (56d), the amplitude of grid errors in physical space due to spectral aliasing for N^3 is one half that for N^1 or N^{41} (Fig. 19). It is clearly seen that the results are not equivalent to those of Fig. 18. Truncation for DF2 (Fig. 20) is much larger than for SL4 (Fig. 21) from the early wave numbers to the cutoff, and it is more significant for N^3 and N^{41} because more derivatives are involved than in N^1. The global error is finally dominated by truncation for DF2 (Fig. 22) and by aliasing for SL4 (Fig. 23), as expected from its high

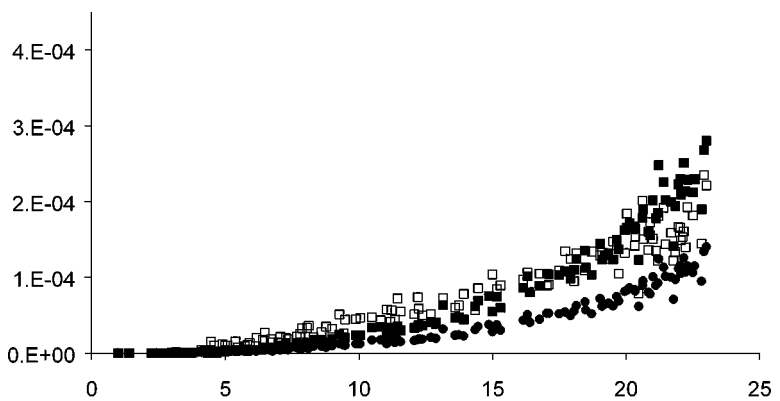

FIG. 19. Aliasing alone. ■, N^1; ●, N^3; □, N^{41}.

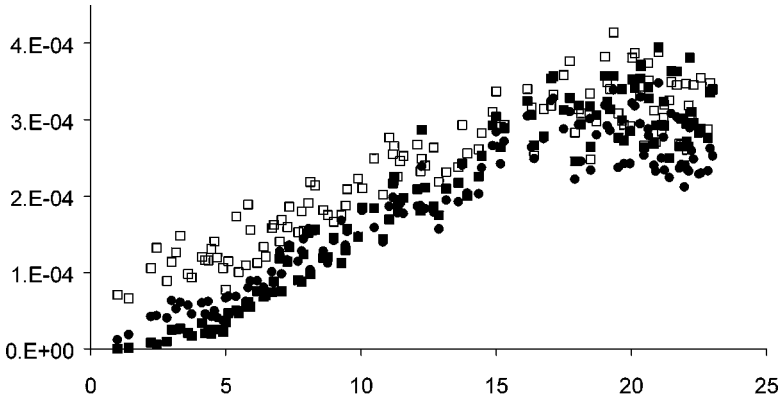

FIG. 20. Truncation alone for DF2. ■, N^1; ●, N^3; □, N^{41}.

resolving efficiency. The couple (N^2, SL4) gives the best global results and the couple (N^1, DF2) gives the worst.

2.5.2. Spectral Transfer. Elimination of the pressure term in the Navier–Stokes equations in spectral space (61) has produced a coupling between the biased projector (60) and the convective terms (57). The results (73) for the form $\tilde{N}'^1$ computed spectrally and with MWNs of DF2 and SL4 are plotted in Fig. 24. The poor resolving efficiency of DF2 damps this transfer in the inertial range and diminishes the production of high wave number modes. On the other hand, the compact scheme produces only little damping of modes very near the cutoff, in the same order of magnitude as dealiasing does for the pseudo-spectral calculation (Fig. 25).

2.5.3. Viscous and subgrid scale dissipation. The diffusion term, $(\nu + \nu^t(k \mid k_c))k''\bar{\tilde{u}}_i(\mathbf{k}, t)$, is governed by the interaction of the subgrid scale model with the errors of the second-order derivation scheme via the product $\nu^t k''$. Once again, the poor resolving efficiency of DF2 (Fig. 26), associated with the "plateau-cusp" model, leads to quite the same result as a spectral or spectral-like scheme associated with a constant subgrid eddy viscosity.

The diffusion term itself is plotted on Fig. 27. Large discrepancies are observed for the second-order scheme, compared to spectral or SL4 schemes. So a question must be

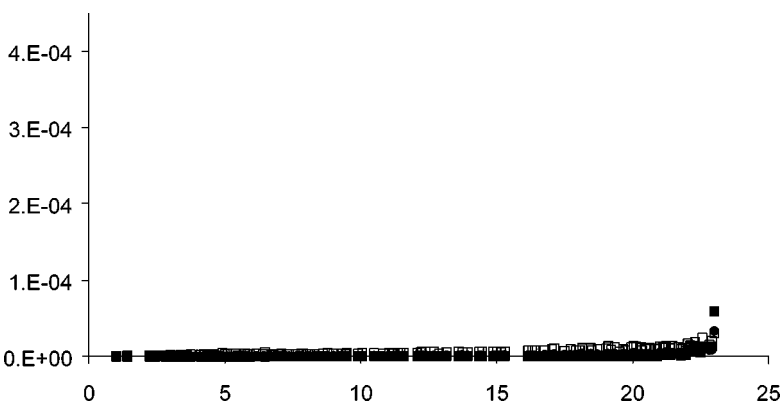

FIG. 21. Truncation alone for SL4. ■, N^1; ●, N^3; □, N^{41}.

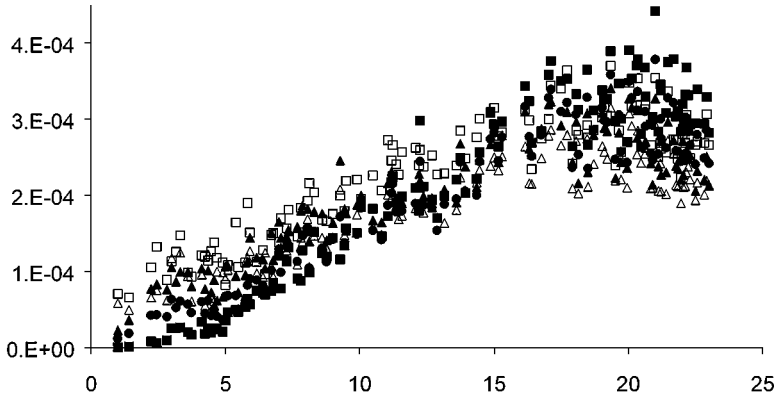

FIG. 22. Global error for DF2. ■, N^1; ▲, N^2; ●, N^3; □, N^{41}; △, N^{42}.

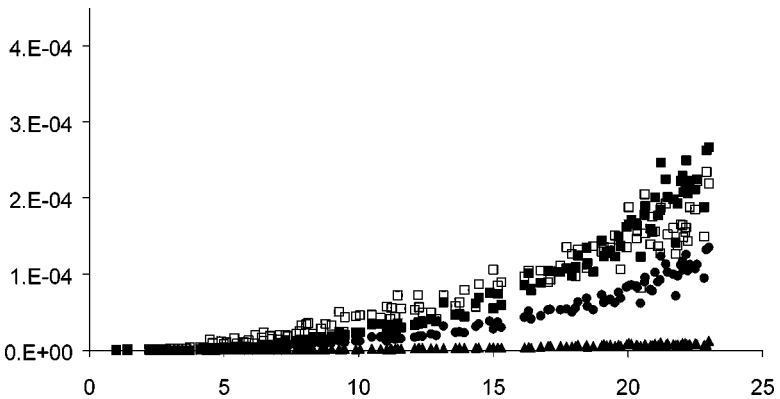

FIG. 23. Global error for SL4. ■, N^1; ▲, N^2; ●, N^3; □, N^{41}; △, N^{42}.

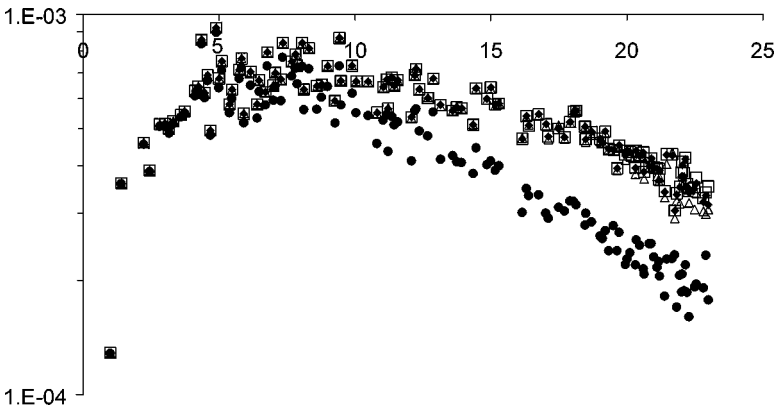

FIG. 24. Spectral transfer (Eq. (73))—form N^1. △, SPDA; □, SP/N1; ◆, SL4/N1; ●, DF2/N1.

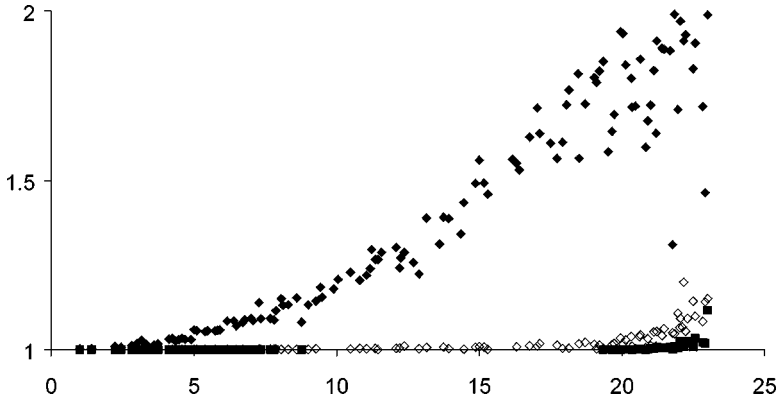

FIG. 25. Ratio of spectral transfers. ◇, SP/SPDA; ◆, SP/DF2; ■, SP/SL4.

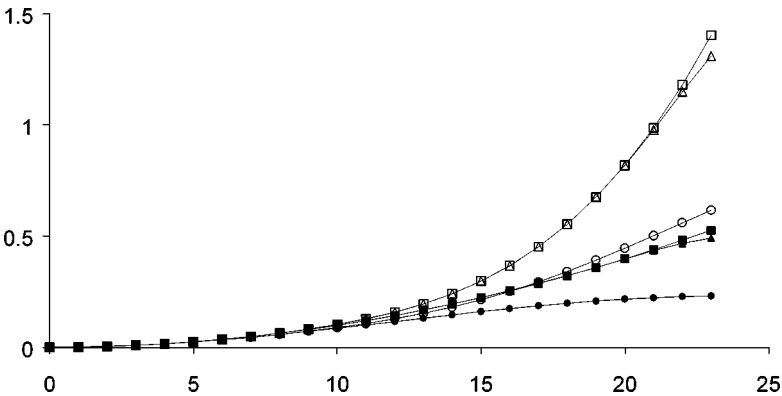

FIG. 26. Nut * k''. ⊟, spectral—cusp; ■, spectral—no cusp; △, SL4—cusp; ▲, SL4—no cusp; ○, DF2—Cusp; ●, DF2—no cusp.

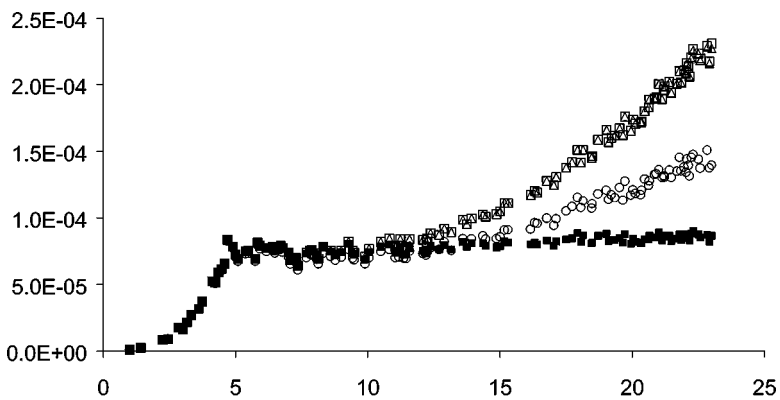

FIG. 27. Diffusion term. □, SP—cusp; ■, SP—no cusp; △, SL4—cusp; ○, DF2—cusp.

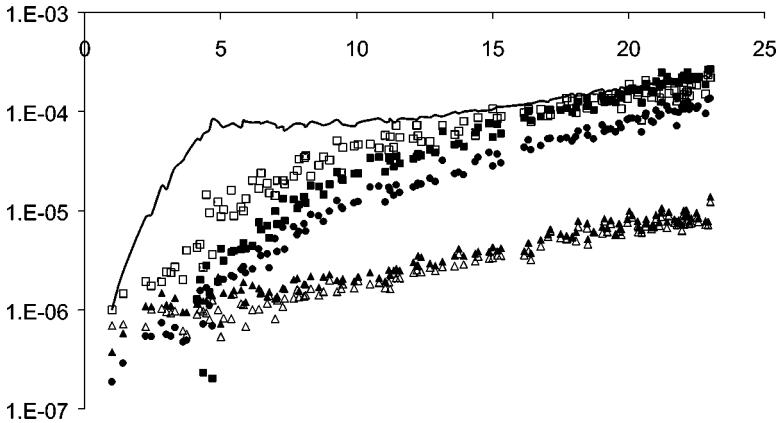

FIG. 28. Total error compared to subgrid term for SL4. —, SGS term—cusp; ■, N^1; ▲, N^2; ●, N^3; □, N^{41}; △, N^{42}.

posed: What sense does low order LES make when the physics introduced in the subgrid modeling is polluted so dramatically? Here, we are dealing with centered, nondissipative finite difference schemes. Therefore, it would be even worse using the so-called MILES approach with monotonic or total variation diminishing (TVD) schemes, as is sometimes done. Nevertheless, in the DNS case where simulated fields have very little energy at the cutoff, the situation may be acceptable.

2.5.4 Total error compared to subgrid term. The total static error is accumulated on the unsteady term $\widetilde{\bar{u}}_{i,t}(\mathbf{k}, t)$ of (71) as the sum of spectral transfer and diffusion errors.

The fourth-order compact scheme error is dominated by aliasing errors for forms N^1, N^3, and N^{41} whose magnitude is comparable to the subgrid diffusion term in the last third of the wave number range. The grid-exact N^2 and N^{42} forms provide excellent low level error over the whole wave number range (Fig. 28).

On the other hand, truncation errors for DF2 overcome the magnitude of the subgrid term for nearly all the wave numbers, independently of the form N^n of the nonlinear terms (Fig. 29). Since for DF2, both spectral transfer (Fig. 24) and subgrid scale dissipation

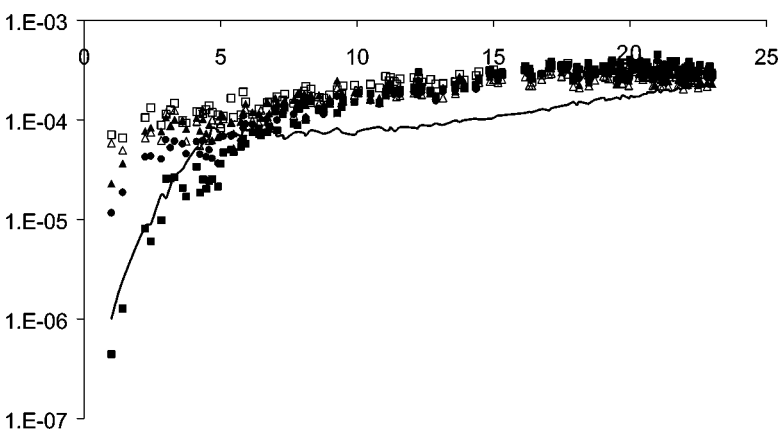

FIG. 29. Total error compared to subgird term for DF2. —, SGS term—cusp; ■, N^1; ▲, N^2; ●, N^3; □,N^{41}; △, N^{42}.

(Fig. 27) are damped from the beginning of the inertial range to the cutoff, a dynamical study is now necessary to see if both effects can compensate each other for long-time integration, i.e., the analysis of stability for total discretization errors.

2.6. *Dynamical Test Case*

We now run the LES of self-decaying homogeneous turbulence at 48^3 resolution with forms N^1 and N^2. The reference calculation is provided by pseudo-spectral dealiased (SPDA) discretization, and comparison is made for DF2 and SL4 finite differences schemes, whose physical space behavior is mimicked by aliased pseudo-spectral calculation with substitution of MWNs in the derivatives. Time stepping is achieved with a second-order Adams–Bashforth (AB2) scheme for nonlinear terms and a Crank–Nicolson implicit scheme for diffusion terms. The initial field is built as described in Section 2.3.2, with an energy spectrum peaking at k_I and a k^n initial infrared range

$$E(k,0) = Ak^n e^{-4(k/k_I)^2}, \qquad A^{-1} = \frac{1}{2}\left(\frac{4}{k_I^2}\right)^{-(n+1)/2} \Gamma\left(\frac{n+1}{2}\right).$$

For the given value of A, the initial normalized kinetic energy k_0 is 1. The initial infrared slope is $n = 8$ and the energetic peak is at $k_I = 8$.

The performances of the schemes to be tested are evaluated from the time evolution of the energy spectrum and associated kinetic energy. Dimensionless time is referred to as large eddy turnover time $(k_0^{1/2} k_I)^{-1}$. An interesting feature of the subgrid scale model (74) is its ability to be inactive as long as the spectrum has no energy at the cutoff. So, one can check, in the early stages of the simulation, the stability of spectral transfer discretization and the emergence of the inertial range independently of the subgrid dissipation, as in Section 1.4. Figure 30 displays the energy spectra at $t = 2$. The inertial range is not yet established and the solution is fully resolved. One can see that the association DF2/AB2 is unstable, mainly with the form N^2 but also with N^1, because of the amplification of all modes.

This is also visible in the early time evolution of the kinetic energy, theoretically conserved by triadic interactions. This behavior is strictly respected by SPDA, whereas DF2/N1 and DF2/N2 produce an amplification by instability and SL4 produces a little damping (Figs. 31 and 32), as already mentioned in [6]. DF2/N2 is more unstable than DF2/N1 because aliasing

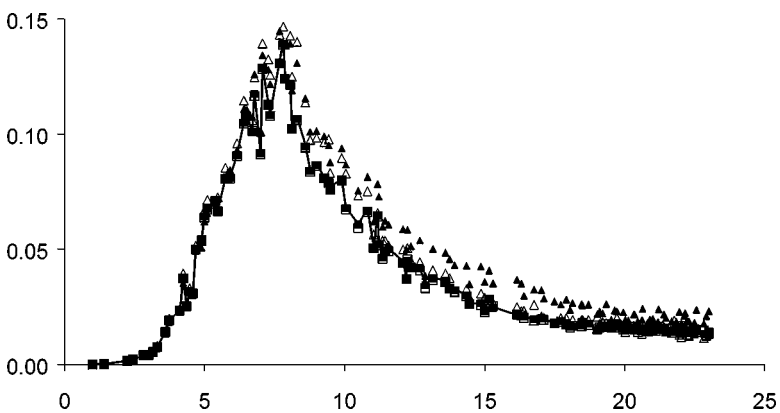

FIG. 30. Energy spectra at $t = 2$. —, SPDA; □, SL4/N1; △, DF2/N1; ■, SL4/,N2; ▲, DF2/N2.

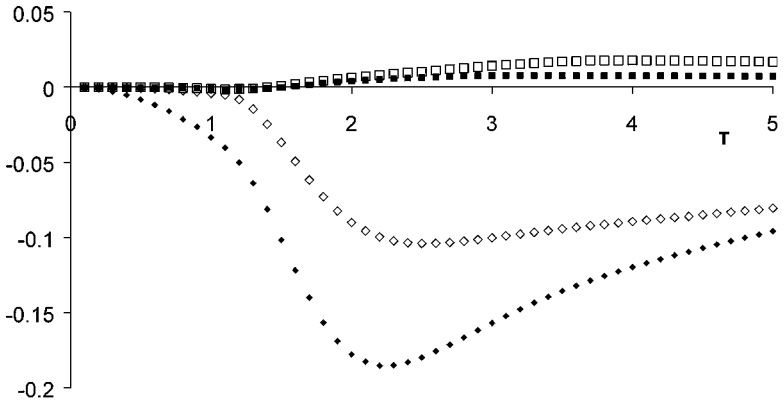

FIG. 31. Time evolution of kinetic energy error. □, SPDA-SL4/N1; ◇, SPDA-DF2/N1; ■, SPDA-SL4/N2; ◆, SPDA-DF2/N2.

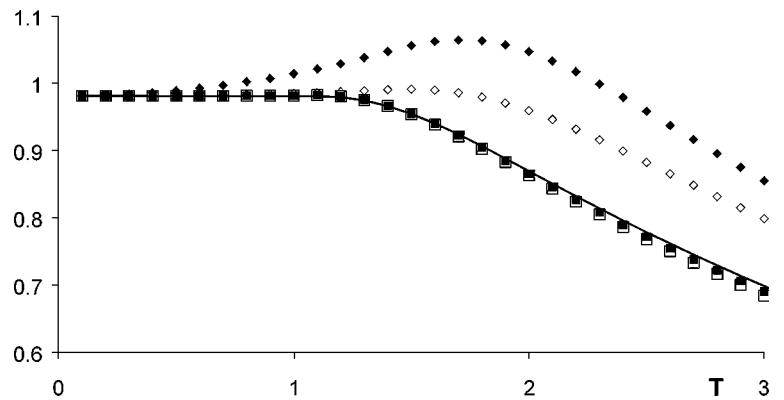

FIG. 32. Early time evolution of kinetic energy. —, SPDA; □, SL4/N1; ◇, DF2/N1; ■, SL4/N2; ◆, DF2/N2.

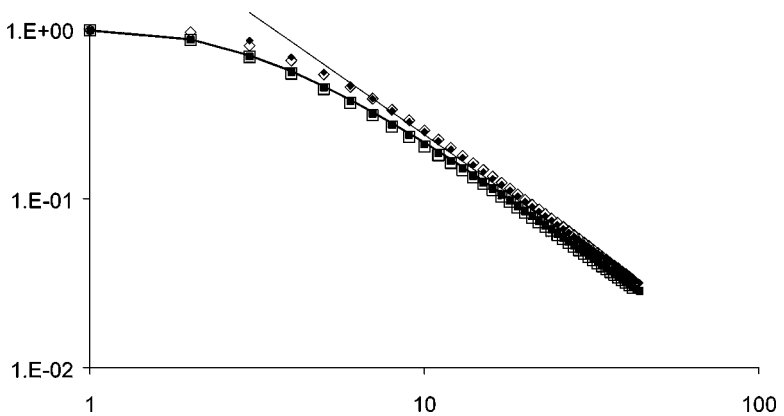

FIG. 33. Time evolution of kinetic energy. —, SPDA; □, SL4/N1; ◇, DF2/N1; ■, SL4/N2; ◆, DF2/N2; —, $t^{-1.38}$.

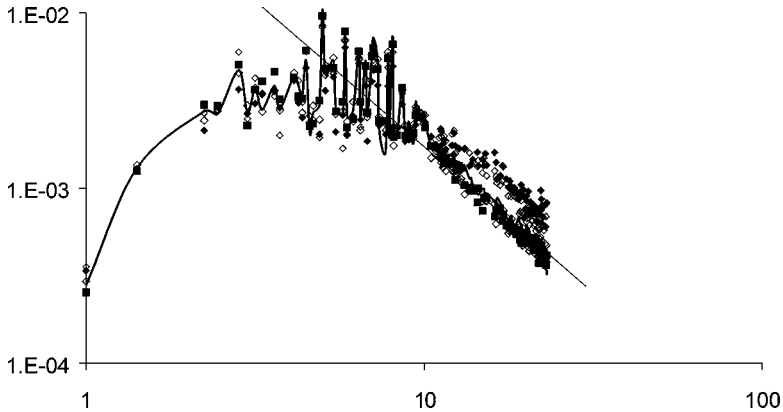

FIG. 34. Energy spectra at $t = 40$. —, SPDA; ◇, SL4/N1; ◇, DF2/N1; ■, SL4/N2; ◆, DF2/N2; —, $k^{-5/3}$.

errors of N^1 are reported mainly at high wave numbers and compensate numerically for the poor MWNs of the scheme.

As soon as the subgrid scale model begins to be active ($t \approx 2.5$), the diffusion term stabilizes DF2, and SL4 tends to reach a similar behavior as SPDA. Finally, at $t = 10$ a very good decay law in $t^{-1.38}$ [15] is observed for SPDA while DF2 and SL4 are still keeping the memory of their initial evolutions but tend to reach asymptotically toward the reference law (Fig. 33), since the dynamical subgrid model adapts itself to numerical errors.

In Fig. 34 the energy spectra for schemes SPDA, DF2, and SL4 are plotted. The dynamic subgrid model provides a slope at the cutoff of about $-5.7/3$ for the reference SPDA, in accordance with previous calculations at higher resolution (64^3 and 128^3) by Lesieur and coworkers [11]. This average value is very sensitive to the range of wave numbers over which the least-squares fit is done to find the exponent m to be put into (762). No attempt has been made to optimize the fitting range (to get closer to $-5/3$); the aim of this study is simply to compare DF2 and SL4 to the reference case SPDA.

So, the dynamical approach permits us to conclude that no error may be *a priori* negligible in an LES due to the high energy level present in the modes near the cutoff, which are mostly affected by aliasing and truncation. Compared to the reference case SPDA, aliasing errors of the divergence form N^1 emphasized by the high resolving efficiency of SL4 produce a slightly different time evolution of the solution. The association SL4/N2 in physical space is nearly equivalent to a dealiased pseudo-spectral calculation. The second-order truncation of DF2 associated with time stepping makes the global scheme unstable for the hyperbolic part of the equations. Introduction of subgrid dissipation leads finally to a surprising acceptable balance, which is better than what one would expect with such a low order scheme.

CONCLUSION

In this paper, some issues on numerical errors in direct and large eddy simulations of turbulence have been revisited. The numerical equivalence between physical space implementation of finite difference schemes and spectral space calculations involving the associated modified wave numbers has been discussed for nonlinear PDEs in divergence or convective forms. It has been shown that only aliased pseudo-spectral calculations can

reproduce the errors at grid points in physical space. The suitable procedure, using a pseudo-spectral code with MWNs instead of wave numbers in derivatives, has then been established for the analysis of truncation errors, aliasing errors, and combination of both in the finite difference LES of turbulent flows.

This procedure has been applied to self-decaying homogeneous isotropic turbulence. Static numerical errors have been evaluated for second-order and highly resolving sixth-order compact finite difference schemes, for all forms of nonlinear terms in the Navier–Stokes equations. Conclusions are as follows:

- Physical space implementation of low-order/resolving efficiency schemes produces a numerical error dominated by truncation whatever form is used.
- Highly resolving schemes emphasize aliasing errors and should be used in conjunction with convective forms.

An interpolation technique in physical space has been proposed to reduce at reasonable cost the numerical errors of the divergence form at grid points. Whether it is worth implementing it in practical simulations depends on the conservative properties required for the discretized equations.

ACKNOWLEDGMENT

We are grateful to Prof. Pierre Sagaut, researcher at French aerospace office O.N.E.R.A., for his fruitful comments on the initial manuscript.

REFERENCES

1. B. J. Boersma and S. K. Lele, Large eddy simulation of compressible turbulent jets, Annual Research Briefs (Center for Turbulence Research, 1999), p. 365.
2. C. Canuto *et al.*, *Spectral Methods in Fluid Dynamics* (Springer-Verlag, Berlin, 1988).
3. B. Fornberg and M. Ghrist, Spatial finite difference approximation for wave-type equations, *SIAM J. Numer. Anal.* **37**, 105 (1999).
4. S. Ghosal, An analysis of numerical errors in large-eddy simulations of turbulence, *J. Comput. Phys.* **125**, 187 (1996).
5. R. H. Kraichnan, Eddy viscosity in two and three dimensions, *J. Atmos. Sci.* **33**, 1521 (1976).
6. A. G. Kravchenko and P. Moin, On the effect of numerical errors in large-eddy simulations of turbulent flows, *J. Comput. Phys.* **131**, 310 (1997).
7. S. K. Lele, Compact finite difference schemes with spectral like resolution, *J. Comput. Phys.* **103**, 16 (1992).
8. M. Lesieur, *Turbulence in Fluids* (Martinus Nijhoff, 1987).
9. T. Lund, On the Use of Discrete Filters for Large Eddy Simulation, Annual Research Briefs (Center for Turbulence Research, 1997), p. 83.
10. O. Metais and M. Lesieur, Spectral large eddy simulation of isotropic and stably stratified turbulence, *J. Fluid Mech.* **239**, 157 (1992).
11. M. Lesieur and O. Metais, New trends in large eddy simulations, *Annu. Rev. Fluid Mech.* **28**, 45 (1996).
12. P. Moin and K. Mahesh, Direct numerical simulation: A tool in turbulence research, *Annu. Rev. Fluid Mech.* **30**, 539 (1998).
13. F. Montigny-Rannou, Influence de l'effet d'aliasing sur la résolution numérique des équations de Navier–Stokes par méthodes spectrales, *Rech. Aerosp.* **2**, 93 (1982).
14. Y. Morinishi, T. Lund, O. Vasilyev, and P. Moin, Fully conservative higher order finite difference schemes for incompressible flow, *J. Comput. Phys.* **143**, 90 (1998).

15. S. A. Orszag, Analytical theories of turbulence, *J. Fluid Mech.* **41**, 363 (1970).
16. T. J. Poinsot and S. K. Lele, Boundary conditions for direct numerical simulations of compressible viscous flows, *J. Comput. Phys.* **101**, 104 (1992).
17. W. Shyy, M. H. Chen, R. Mittal, and H. S. Udaykumar, On the suppression of numerical oscillations using a non linear filter, *J. Comput. Phys.* **102**, 49 (1992).
18. O. Vasilyev, On the Construction of high order Finite Difference Schemes on non-uniform Meshes with good Conservation Properties, Annual Research Briefs (Center for Turbulence Research, 1998), p. 311.
19. G. B. Whitham, *Linear and Non linear Waves* (Wiley, New York, 1974).